Electrochimica Acta 412 (2022) 140072

Contents lists available at ScienceDirect

Electrochimica Acta

journal homepage: www.journals.elsevier.com/electrochimica-acta

Disentangling faradaic, pseudocapacitive, and capacitive charge storage: A tutorial for the characterization of batteries, supercapacitors, and hybrid systems

T. Schoetz [a], L.W. Gordon [a], S. Ivanov [b], A. Bund [b], D. Mandler [c], R.J. Messinger [a,*]

[a] Department of Chemical Engineering, The City College of New York, CUNY, 160 Convent Ave., New York, NY 10031, USA
[b] Electrochemistry and Electroplating Group, Technische Universität Ilmenau, Ilmenau 98693, Germany
[c] Institute of Chemistry, The Hebrew University of Jerusalem, Jerusalem 9190401, Israel

A B S T R A C T

Today's electrochemical energy storage technologies aim to combine high specific energy and power, as well as long cycle life, into one system to meet increasing demands in performance. These properties, however, are often characteristic of either batteries (high specific energy) or capacitors (high specific power and cyclability). To merge battery- and capacitor-like properties in a hybrid energy storage system, researchers must understand and control the co-existence of multiple charge storage mechanisms. Charge storage mechanisms can be classified as faradaic, capacitive, or pseudocapacitive, where their relative contributions determine the operating principles and electrochemical performance of the system. Hybrid electrochemical energy storage systems can be better understood and analyzed if the primary charge storage mechanism is identified correctly. This tutorial review first defines faradaic and capacitive charge storage mechanisms and then clarifies the definition of pseudocapacitance using a physically intuitive framework. Then, we discuss strategies that enable these charge storage mechanisms to be quantitatively disentangled using common electrochemical techniques. Finally, we outline representative hybrid energy storage systems that combine the electrochemical characteristics of batteries, capacitors and pseudocapacitors. Modern examples are analyzed while step-by-step guides are provided for all mentioned experimental methods in the Supplementary Information.

1. Introduction

When can a lithium-ion battery be classified as a "hybrid system"? What is pseudocapacitance and how can it be identified and distinguished electrochemically? These questions and more arise with today's electrochemical energy storage systems, which may combine a mix of charge storage mechanisms and thereby blur the boundaries between batteries and capacitors.

Notably, electrochemical performance metrics are mechanism specific. Hybrid energy storage systems with overlapping charge storage mechanisms can easily be mischaracterized when the primary charge storage mechanism is not identified correctly. Correct characterization has implications on how researchers interpret experimental data and assign electrochemical performance metrics. For example, an electrochemical charge storage system might be classified as a 'capacitor' when it is in fact a 'battery', which might occur when significant pseudocapacitive contributions are present. Once the charge storage mechanisms are correctly identified, then researchers can better understand and control material properties and experimental conditions to minimize trade-offs between performance-related parameters such as energy or power per mass or volume, capacity, capacitance, and cycle life.

Standard electrochemical characterization techniques such as cyclic voltammetry, constant current (galvanostatic) cycling, and electrochemical impedance spectroscopy do not distinguish the underlying mechanisms of hybrid systems without deeper analysis. For this reason, multiple experimental methods or analyses must be combined strategically to describe unambiguously the charge storage mechanisms and quantify their relative contributions to the overall capacity.

This tutorial review provides an overview of faradaic, capacitive, and pseudocapacitive charge storage mechanisms in electrochemical energy storage systems and practical strategies to identify, characterize and quantitatively disentangle them. Researchers can distinguish these charge storage mechanisms using common electrochemical methods such as variable-rate cyclic voltammetry, galvanostatic cycling, potential step methods, and electrochemical impedance spectroscopy. In the following, we outline the necessary theoretical background to apply these experimental techniques to distinguish charge storage mechanism in hybrid energy storage systems, along with modern examples from the literature and key references for further reading [1–10]. Step-by-step guides are provided for all mentioned experimental methods in the

* Corresponding author.
E-mail address: rmessinger@ccny.cuny.edu (R.J. Messinger).

https://doi.org/10.1016/j.electacta.2022.140072
Received 12 October 2021; Received in revised form 14 February 2022; Accepted 14 February 2022
Available online 15 February 2022

Supplementary Information.

1.1. Charge Storage Mechanisms

Today's electrochemical energy storage systems and devices, both mobile and stationary, often combine different charge storage mechanisms whose relative contributions are rate dependent (Fig. 1). Physically, charge storage mechanisms can be classified into two categories: *capacitive* and *faradaic* (Fig. 1). Both charge storage mechanisms differ by their root cause for storing charge; in addition, they differ by how mass transfer affects their rates. Capacitive charge storage results from the physical separation of charges at the interface of an electrode. An *electric capacitor* consists of electrodes with an electrically insulating but polarizable dielectric between them. When a potential difference is applied and charges of opposite sign accumulate on the opposing electrodes, charge is locally compensated by polarization of the dielectric, but charge-compensating ion mass transfer does not occur between them. *Supercapacitors* consist of high-surface area porous electrodes with an ion-containing electrolyte between them. Upon application of a potential difference, electrode charge compensation involves molecular rearrangements on the scale of the *electrical double layer*, which is usually on the order of a nanometer; rates are not governed by ion mass transfer at these scales and are thereby *capacitive non-diffusion-limited*. Faradaic charge storage occurs due to an electrochemical redox reaction at the electrode-electrolyte interface, across which electrons (charges) are transferred. The redox reaction requires the mass transfer of ions to the interface, and in the two limiting cases, can either be *faradaic diffusion-limited* or *faradaic non-diffusion-limited*. The latter describes *pseudocapacitive* charge storage, which will be more rigorously defined below.

2. Mass transport and electrochemical kinetics

For faradaic charge storage, an electrochemical redox reaction occurs at the electrode-electrolyte interface, whose "overall" rate depends upon the interplay between ion mass transfer in the electrolyte and electrochemical kinetics at the electrode.

2.1. Rate of mass transport

Mass transport of ionic species in an electrochemical system is given by three different driving forces: diffusion, electromigration, and convection. The mass flux of an ionic species, *J*, within a dilute electrolyte can be expressed by the Nernst-Planck equation: [2,11].

$$J = \underbrace{-D\nabla c}_{\text{Diffusion}} \underbrace{-\frac{zF}{RT}Dc\nabla\varphi}_{\text{Migration}} + \underbrace{cu}_{\text{Convection}} \quad (1)$$

The first term is the mass flux due to *diffusion,* where macroscopic ion mass transport occurs due to random molecular motions down a concentration gradient -∇c with a diffusion constant *D*. The second term is the mass flux due to ionic *migration*, where ions are forced along an electric field -$\nabla\varphi$, where φ is the electric potential. The expression for migration also contains the ion charge number, *z*, Faraday's constant, *F*, the universal gas constant, *R,* and the temperature, *T*. The third term is the mass flux due to *convection*, where ions are advected by the surrounding fluid moving with a velocity *u*.

To simplify, we neglect convection, as many electrochemical energy storage devices do not involve mixing or pumping of the electrolyte (a notable exception being redox flow batteries [12]). Natural convection due to differences in fluid density, which may arise due to concentration gradients generated during electrochemical reactions as well as any temperature gradients, is often negligible. Note that convection does not occur in solid electrolytes. In addition, we consider systems where ion migrative transport due to potential gradients $\nabla\varphi$ is small compared to diffusive transport. Ion migration can typically be neglected when charge-transporting ion species are surrounded by an excess of supporting electrolyte that does not participate in the electrode reactions, or in electrolytes with high conductivity where the electric field is small in the bulk electrolyte. Therefore, the Nernst-Planck equation (Eq. (1)) simplifies to $J_{diff} = -D\nabla c$, also known as Fick's first law of diffusion. Using molar units, we equate the mass flux, with dimensions of moles per unit area per unit time (e.g., mol cm^{-2} s^{-1}) to a rate of diffusion, $r_{diff} \equiv J_{diff}$, which is proportional to the concentration gradient, $r_{diff} \sim \nabla c$.

In certain electroactive materials that store charge faradaically, such as battery intercalation electrodes, mass transport of ions can occur both to, and within, the solid electrodes. We highlight that the transport of ions within the electrolyte to an electrode surface (e.g., Li^+ diffusion to metallic Li during electroplating) as well as the transport of ions within a solid-state material (e.g., Li^+ diffusion in graphite after electrochemical intercalation) can both play a critical role in controlling the experimentally observed current density. However, in both cases, ion diffusion relates to their statistical movement down a concentration gradient, -∇c. This concentration gradient may be present in the electrolyte at the electrode-electrolyte interface, including electrolyte within porous electrode structures, and/or within the solid electrode itself. While

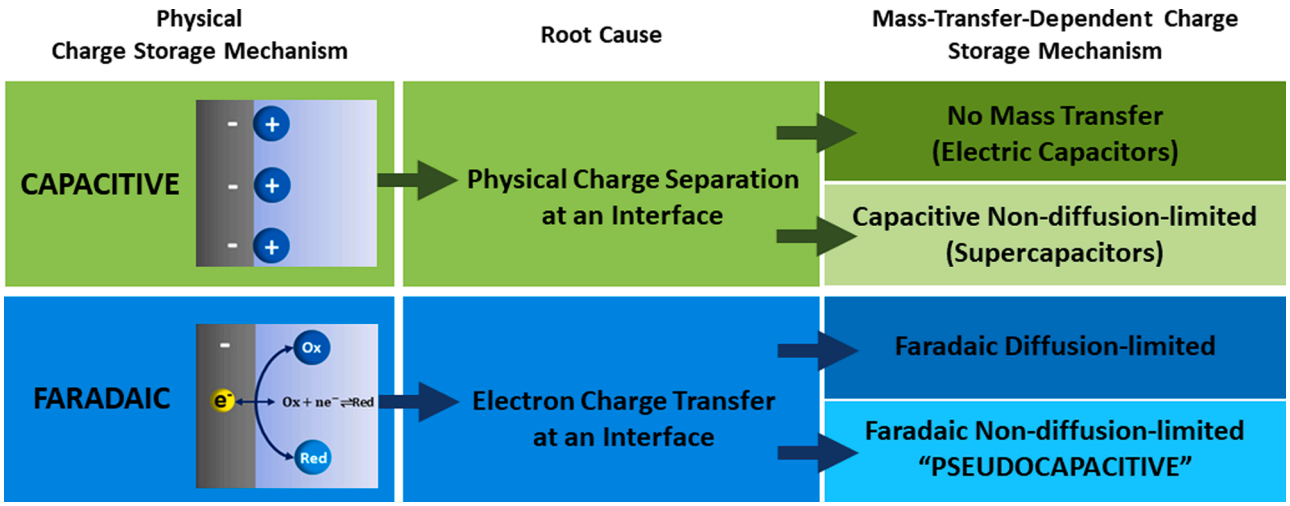

Fig. 1. Capacitive and faradaic charge storage mechanisms distinguished by their root cause and mass transfer regimes. Faradaic charge storage can be diffusion-limited or non-diffusion-limited. The latter is also called "pseudocapacitive" charge storage, which depends upon the relative rates of diffusion and electrochemical reaction.

electrochemical characterization methods alone cannot typically distinguish between these different diffusional processes, they can determine whether ion diffusion (whether in the electrolyte, electrode, or both) limits the current response through quantitative scaling relationships, as shown below. Regardless of the origin of the concentration gradient(s) and resulting diffusion limitations, in such electrochemical systems, the rate r_{diff} is often controlled by ion diffusion in one phase where it is rate limiting.

2.2. Rate of electrochemical reaction

When an electroactive species arrives at the reaction site on the electrode surface, an electrochemical reaction occurs wherein electrons are transferred across the electrolyte-electrode interface, constituting a flux of electrons with an electrochemical reaction rate r_{rxn} according to

$$\mathrm{r_{rxn}} = \frac{\mathrm{j_{rxn}}}{\mathrm{z_e F}} \tag{2}$$

where j_{rxn} is the current density of the electrochemical reaction and z_e is the number of electrons transferred per ion. The rate r_{rxn} has dimensions of moles per unit area per unit time (e.g., mol cm^{-2} s^{-1}).

For many common electrochemical systems, the current density associated with the electrochemical charge transfer reaction j_{rxn} can be expressed by the *Butler-Volmer* equation,

$$\mathrm{j_{rxn}} = \mathrm{j_0}\left[\exp\left(\frac{\alpha_a \mathrm{F}}{\mathrm{RT}}\eta_{ct}\right) - \exp\left(-\frac{\alpha_c \mathrm{F}}{\mathrm{RT}}\eta_{ct}\right)\right] \tag{3}$$

where j_0 is the *exchange current density*, η_{ct} is the *charge-transfer overpotential*, and α_a and α_c are the anodic and cathodic *transfer coefficients*. The charge-transfer overpotential associated with electron charge transfer across the interface is defined as $\eta_{ct} = \mathrm{E} - \mathrm{E_{eq}}$, where E is the potential of the electrode and E_{eq} is the equilibrium potential as defined by the Nernst equation [2,11]. The exchange current density j_0 reflects the intrinsic rate of electron transfer across the interface and is analogous to the rate constant used in chemical kinetics. However, unlike kinetic rate constants, j_0 depends upon the concentrations of the reactants and products, in addition to the temperature and the nature of the interface. The higher the exchange current density, the faster the electrode reaction. The exponential terms $\mathrm{j_0}\exp\left(\frac{\alpha_a \mathrm{F}}{\mathrm{RT}}\eta_{ct}\right)$ and $\mathrm{j_0}\exp\left(-\frac{\alpha_c \mathrm{F}}{\mathrm{RT}}\eta_{ct}\right)$ are the anodic and cathodic currents, respectively, and are analogous to forward and backward reactions in chemical kinetics. The difference between the anodic and cathodic currents sets the direction of the reaction and hence the current density. The transfer coefficients α_a and α_c are linked to the symmetries of the anodic and cathodic reactions, respectively.

More generally, electrochemical reactions may involve a sequence of elementary steps, such as single electron transfer reactions, adsorption and desorption steps, surface diffusion and crystallization, or (heterogeneous or homogeneous) chemical reactions that occur immediately preceding or following the electrochemical reaction. When the elementary steps are known, the kinetics of each step must be considered. Depending on the complexity of the reaction mechanism, and to the extent that one step is rate limiting, the "apparent" electrochemical kinetics of the reaction sequence may or may not be described in a Butler-Volmer-like form [11]. In addition, surface processes, such as adsorption, surface diffusion, or crystallization, may be modeled as having associated overpotentials η_i. Here, we define the *activation overpotential* $\eta_a = \eta_{ct} + \sum \eta_i$ as the overpotential necessary to drive the electrochemical reaction, including any such surface processes. For electrochemical reactions involving only a simple electron transfer, or when such a step is rate limiting, the activation potential is equivalent to a charge-transfer overpotential, $\eta_a = \eta_{ct}$.

Thus, the current density of the "apparent" electrochemical reaction, j_{rxn}^{app}, which includes all elementary reaction steps and surface processes, is defined by:

$$\mathrm{j_{rxn}^{app}} = \mathrm{j_0}\left[\exp\left(\frac{\alpha_a \mathrm{F}}{\mathrm{RT}}\eta_a\right) - \exp\left(-\frac{\alpha_c \mathrm{F}}{\mathrm{RT}}\eta_a\right)\right] \tag{4}$$

The "apparent" electrochemical rate is thus:

$$\mathrm{r_{rxn}^{app}} = \frac{\mathrm{j_{rxn}^{app}}}{\mathrm{z_e F}} \tag{5}$$

The activation overpotential η_a is a driving force for the electrochemical reaction, which is controlled experimentally by altering the potential E of the electrode and hence the electrochemical potential (energy level) of its electrons. When $\mathrm{E} = \mathrm{E_{eq}}$, the system is in a state of dynamic equilibrium: the anodic and cathodic currents balance, the surface concentrations of the electroactive species just outside of the electric double layer correspond to their bulk values, and the net current density is zero. When the overpotential is small ($|\eta_a| \ll \frac{\mathrm{RT}}{\mathrm{F}}$), the current scales linearly with the overpotential. When the overpotential is large ($|\eta_a| \gg \frac{\mathrm{RT}}{\mathrm{F}}$), either the anodic or cathodic current will dominate, depending on the sign of η_a, which leads to a current with an exponential dependence on overpotential. This limit is known as the Tafel relationship. Systems with large overpotentials, $|\eta| > 118$ mV at 25 °C, are often well described by the Tafel plots [2,13].

A fundamental microscopic theory describing electron transfer kinetics was developed by Marcus, which can be used in place of the Butler-Volmer relationship (Eq. (3)) [2,14,15]. Marcus theory [16,17] and its subsequent developments describe electron transfer reactions using expressions grounded in quantum mechanics and statistical mechanics. This approach can be more accurate for certain electrochemical systems (e.g., electron transfer during Li^+ intercalation into carbon-coated Li_xFePO_4) [14,15].

2.3. Interplay between rates of mass transport and electrochemical reaction

In practice, in an electrochemical experiment—including the charging or discharging of an electrochemical energy storage device—the current density j that is measured experimentally is equivalent to an "overall" rate of the electrochemical reaction that depends on both mass transport and electrochemical kinetics. The experimental current density j depends upon the *total overpotential*, η, according to

$$\mathrm{j} = \mathrm{j_0}\left[\exp\left(\frac{\alpha_a \mathrm{F}}{\mathrm{RT}}\eta\right) - \exp\left(-\frac{\alpha_c \mathrm{F}}{\mathrm{RT}}\eta\right)\right] \tag{6}$$

Here, $\eta = \eta_a + \eta_c$, where η_c is the *concentration overpotential* associated with concentration gradients ∇c in the electrolyte generated by operating the electrochemical cell. The concentration overpotential depends also upon the ion transference numbers, or the fraction of current that each ion carries in the solution.

These competing rate processes can be encapsulated within a dimensionless parameter. We define a general electrochemical Damköhler number, Da_{el}, that quantifies the relative contributions of the "apparent" electrochemical rate of reaction, r_{rxn}^{app}, which includes all surface processes, and the overall rate of diffusion, r_{diff}:

$$\mathrm{Da_{el}} = \frac{\mathrm{r_{rxn}^{app}}}{\mathrm{r_{diff}}} \tag{7}$$

Da_{el} thus encapsulates the ratio of the rates of electrochemical reaction and diffusion, i.e., the electrochemical reactive flux to the diffusive flux. If desired, r_{diff} can be generalized to an overall rate of mass transfer, r_m, that includes include ion migration and/or convection (Eq. (1)), as discussed above. Notably, while the rate of the electrochemical reaction r_{rxn}^{app} depends upon the intrinsic physical, chemical, and electronic nature of the system, it can also be altered by changing the potential E of the electrode. Similarly, the rate of diffusion r_{diff} depends not

only upon the system but also the experimental parameters because any ion concentration gradients ∇c that develop will depend upon, e.g., the rate of charge or discharge. Thus, Da_{el} is both system- and experiment-dependent. When

$$Da_{el} \gg 1 \text{ or } r_{rxn}^{app} \gg r_{diff}, \quad (8)$$

the system is *diffusion-limited*: the rate of diffusion is much less than the rate of electrochemical reaction. Electrochemical energy storage systems in this regime are *faradaic diffusion-limited* (Fig. 1). Conversely, when

$$Da_{el} \ll 1 \text{ or } r_{rxn}^{app} \ll r_{diff}, \quad (9)$$

the system is *reaction-limited*: the rate of electrochemical reaction is much less than the rate of diffusion. Electrochemical energy storage systems in this regime are *faradaic non-diffusion-limited*, which we define as *pseudocapacitive* (Fig. 1).

In the intermediate or "mixed" regime ($Da_{el} \sim 1$), both ion mass transport and electrochemical kinetics dictate the overall rate of reaction and hence the experimental current density, j. Such intermediate regimes may occur over common experimental conditions in hybrid electrochemical energy storage devices designed to function at "fast" rates or exhibit significant pseudocapacitive character. In fact, most devices with significant pseudocapacitive contributions are not purely reaction-limited ($Da_{el} \ll 1$) but operate in a mixed regime where ion diffusion still plays a role in controlling the current density. However, it is instructive to explore the extreme limits.

Analyzing the extreme limits of this framework, as quantified by Da_{el}, reveals "speed limits" for electrochemical energy storage systems that store charge faradaically, such as batteries. The first speed limit occurs when the system is completely reaction-limited ($Da_{el} \ll 1$). Then, the experimental current density j is limited by the rate of the electrochemical reaction, j_{rxn}^{app} (i.e., $j = j_{rxn}^{app}$). Unless the pathway is fundamentally altered (e.g., catalytically), the reaction cannot occur faster under a given set of conditions (e.g., temperature, potential, etc.). In this regime, the concentration of the reactants at the electrode surface is equal to the bulk concentration, as no concentration gradients form, and ion mass transport plays no role in dictating the current density. Instead, the current density (Eq. (4)) due to the rate of electrochemical reaction (Eq. (5)) is linked to the frequency of attempts (e.g., due to random molecular collisions and Brownian motion) and the probability of success (e.g., activation energy) of the rate-limiting step. Note that the electrochemical reaction rate is a fundamental limit—mass transfer to the electrode surface can only slow down the "overall" rate of the electrochemical reaction.

Depending on the nature of the system and experimental parameters, the electrochemical reaction is often fast compared to mass transport, and thus ion diffusion plays a key role in controlling the overall current density. The second speed limit occurs when the system is completely diffusion-limited ($Da_{el} \gg 1$). Then, the experimental current density j is rate-limited by the diffusive flux of ions to the electrode, ultimately resulting in a *limiting current* j_{lim} (i.e., $j = j_{lim}$). In this regime, the concentration of the reactants adjacent to the electrode surface is zero, while the current density does not depend upon any kinetic parameters. Instead, the ions react as soon as they reach the electrode surface. The current density cannot be increased further without enhancing the mass flux of ions to the electrode surface, e.g., by convection.

The interplay between mass transfer and electrochemical kinetics, whose regimes are encapsulated by Da_{el}, can be distinguished quantitatively using common electrochemical methods, as shown below. Simple quantitative scaling relationships are particularly insightful for understanding the regime over experimental conditions of interest.

3. Physical charge storage mechanisms

The physical origins, thermodynamics, and rate-dependent implications of faradaic, capacitive, and pseudocapacitive charge storage mechanisms are discussed in more detail.

3.1. Capacitive charge storage

As mentioned above, capacitive charge storage is based on the physical separation of charges and is *not* accompanied by the transfer of charges across an interface. Upon charging, the charge capacity ΔQ_{cap} stored over a potential window ΔE results in an excess of electrons in one phase and concomitant deficiency in the other, which can be written as

$$\Delta Q_{cap} = C \Delta E \quad (10)$$

that defines the capacitance C, which notably is a constant in an electrochemical system [2,4,6]. Note that ΔQ_{cap} (e.g., in mAh) encapsulates the overall quantity of stored charge and is called 'capacity', whereas the 'capacitance' C (e.g., in F) describes the quantity of accumulated charges over a specified potential difference.

A conventional *electric capacitor* (Fig. 2A) is composed of two electrodes divided by a dielectric. The dielectric is an electrically insulating but polarizable material, which is commonly glass, ceramic, a polymer, air, or an oxide layer. When a potential is applied, charges of the dielectric orientate towards the opposed electrodes, generating a flow of electrons through the external source circuit to charge balance each interface. However, no ionic or molecular mass transfer occurs between the electrodes because of the insulating dielectric [2,4,6].

An *electrical double layer capacitor* (EDLC), also known as a *supercapacitor* (Fig. 2B), does not have a dielectric but is composed of an electrolyte with solvated anions and cations between the electrodes. When a potential is applied, solvated ions of opposite charge accumulate at each polarized electrode, forming a charge-balancing electrical double layer. At equilibrium, the charge of the polarized electrode, $Q_{Electrode}$, is counterbalanced by ions in the electrolyte, $Q_{Electrolyte}$. The dielectric, in this case, is the solvation shell of each ion in the electrolyte. Electrodes of supercapacitors (e.g., activated carbon) are usually porous and have very high specific surface areas, which increase charge density and consequently the capacitance and specific power of the device. The prefix 'super' in supercapacitors is based on the fact that the capacitance of supercapacitors can be over 3 orders-of-magnitude greater than conventional electric capacitors [2,4,6].

In comparison to systems with faradaic charge storage, capacitors and supercapacitors can achieve much higher rate capabilities and exhibit much higher specific power because they are not subject to diffusion limitations. EDLCs can charge and discharge at rates associated with the fast formation and dismantling of the electric double layer, on the order of 10^{-6} s, enabling the capacitive device to charge and discharge up to 1000 times faster than a typical faradaic system. In addition, because there are no chemical and structural changes associated with electrochemical redox reactions, the charge and discharge processes are remarkably reversible, resulting in ultra-long cycle lives. However, the specific energy of capacitors is lower than in faradaic charge storage systems, such as batteries, because charge is only stored at the interface and not in ionic or chemical bonds associated with electrochemical intercalation or conversion reactions [2,4,6,18].

3.2. Faradaic charge storage

Faradaic charge storage is defined by the transfer of electrons across an interface, where the charge transfer is based on an electrochemical redox reaction $Ox + z_e \rightleftharpoons Red$, that causes a faradaic current, i_{farad}, to flow. The total quantity of charge transferred Q_{farad} (or faradaic stored capacity) over a time, t, is governed by Faraday's law:

$$Q_{farad} = \int i_{farad}\, dt = n z_e F \quad (11)$$

where n is the number of moles, z_e is the stoichiometric number of

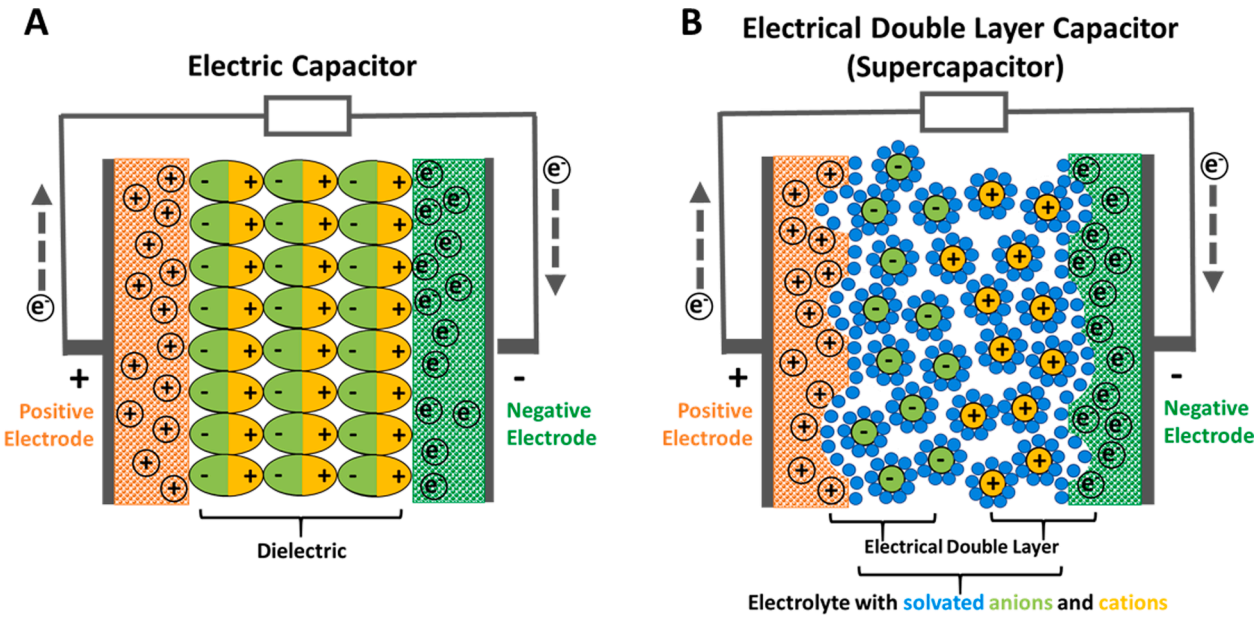

Fig. 2. Schematic of (A) an electric capacitor with a dielectric and (B) an electrical double layer capacitor (supercapacitor) with an electrolyte.

electrons involved in an electrode reaction and F is the Faraday constant [2].

The electrode-electrolyte interface in a faradaic charge storage system, such as a battery, is similar to a supercapacitor (Fig. 2B), raising the question of whether a faradaic system has a capacitance, C, since it also has an electrical double layer. Every electrode-electrolyte interface, whether in a capacitive or faradaic charge storage system, indeed forms an electric double layer that is described by the *electrical double layer capacitance,* C_{DL}. This double layer capacitance can be mostly neglected in faradaic energy storage devices as it does not contribute significantly to the overall charge storage capacity. Typically, C_{DL} is in the range of 10 to 40 μF cm^{-2} in batteries with predominantly faradaic diffusion-limited charge storage. The structure of the electrical double layer can be described by the Helmholtz, Gouy-Chapman and Stern models [19]; the double layer has been analyzed and reviewed extensively elsewhere [2].

3.2.1. *Pseudocapacitive charge storage*

For both faradaic diffusion-limited and faradaic non-diffusion-limited charge storage, the electroactive species undergoes a redox reaction at the electrode-electrolyte interface. However, both processes are distinguished by their respective diffusion rates, r_{diff}, relative to the rate of the redox reaction, r_{rxn}^{app}, as quantified by Da_{el} Eqs. (7)–((9)).

Pseudocapacitive charge storage (Fig. 3) occurs when mass transport of the electroactive species to the electrode surface is much faster than the rate of the electrochemical redox reaction ($Da_{el} \ll 1$ or $Da_{el} \sim 1$). Note that the electroactive species will also form a transient electrochemical double layer with an associated apparent capacitance "C_{pseudo}", analogous to a capacitive system, at the polarized electrode surface. However, charge transferred across the interface is faradaic in nature, resulting from an electrochemical redox reaction that cannot be characterized by a constant capacitance. Pseudocapacitance is therefore a macroscopic charge storage phenomenon of an electrochemical system whose signature of the current response in an electrochemical experiment appears similar to a conventional capacitor but is, in fact faradaic in nature [4,6,20]. This appearance leads to the term 'pseudocapacitance'. The prefix 'pseudo' originates from the Greek language 'psevdís', which can be interpreted as 'looks or appears like' [6].

Based on this framework, we assert that that a pseudocapacitive system *cannot* have a so-called capacitance "C_{pseudo}" since the root cause of the charge storage mechanism is faradaic and thus it would be a function of the potential due to the occurring redox reaction. *Ergo*, "C_{pseudo}" would not be constant as in a capacitive charge storage system.

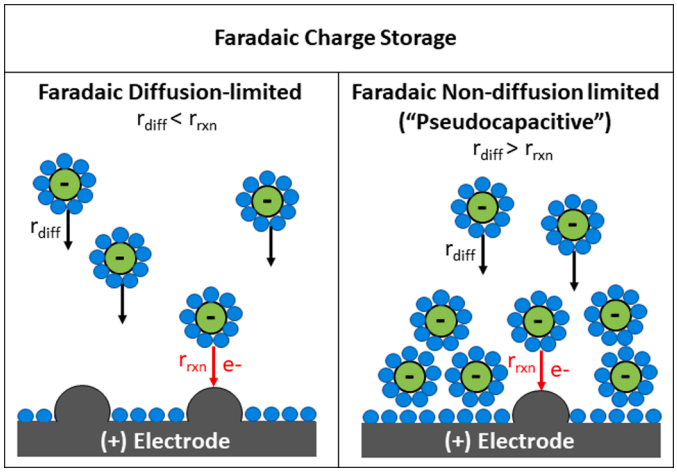

Fig. 3. Schematic illustration of faradaic charge storage mechanisms, which can either be faradaic diffusion-limited or faradaic non-diffusion-limited ("pseudocapacitive").

Pseudocapacitive materials can show electrochemical properties similar to supercapacitors, such as a fast-charging capabilities, because the reactions occurring at the interface are not completely diffusion-limited. Faradaic reactions associated with the electrochemical adsorption of ions, or certain electrochemical surface reactions, are often pseudocapacitive in nature as they are not controlled by ion diffusion. Therefore, systems with primarily pseudocapacitive charge storage are often called fast-charging batteries. Moreover, systems using pseudocapacitive charge storage are often associated with higher specific power than systems with faradaic diffusion-limited charge storage, while exhibiting higher specific energy than capacitors [10].

4. Electrochemically distinguishing and disentangling charge storage mechanisms

This section provides a guide on how to perform and analyze electrochemical methods to distinguish between capacitive, faradaic, and pseudocapacitive charge storage, including cyclic voltammetry (CV) or

linear sweep voltammetry (LSV), potential step methods (chronocoulometry and chronoamperometry), galvanostatic charge/discharge cycling (chronopotentiometry), and electrochemical impedance spectroscopy (EIS).

4.1. Cyclic voltammetry & linear sweep voltammetry

4.1.1. Qualitative interpretation of curve shapes

Potentiodynamic methods such as CV or LSV measure the current that flows through an electrochemical system as the electrode potential is swept over a specified potential window. The qualitative shape of the voltammogram is influenced by the interplay of ion diffusion processes and electrochemical kinetics and thus can suggest the nature of the charge storage process.

A rectangular shape with constant current plateaus and no peaks indicates capacitive charge storage as no redox reaction occurs at the electrode surface that alters the current. The stored charge is directly proportional to the potential window ΔE (Eq. (10)) and the current i scales linearly with the scan rate υ ($i \sim \upsilon$). Thus, for an ideal capacitor, the capacitance C is constant and independent of the potential window. The corners of a CV scan for a capacitor are usually rounded because of resistances in the system that cause a slow rise in the current at the scan's start and reversal. An example CV scan of a supercapacitor, based on carbon nanotubes and graphite nanofiber nanocomposites in 6 mol L^{-1} KOH electrolyte [21], is shown in Fig. 4A.

A CV or LSV curve shows current peaks (sometimes called voltametric waves) when a diffusion-limited redox reaction occurs ($Da_{el} \gg 1$). The peak can be divided into three regimes [22], which can be understood once again by analyzing the interplay between electrochemical kinetics and mass transfer. When the current increases the redox reaction is initially controlled by the kinetics of the electrochemical reaction. However, as the reaction proceeds, the concentration of the electroactive species at the electrode surface continues to be consumed, resulting in an increasing concentration gradient ∇c and a mixed diffusion-reaction regime. When the current reaches its maximum peak current i_p, the concentration of electroactive species at the electrode surface is depleted and the current enters a completely mass-transfer-limited regime. As the potential is swept further, the current then decreases because the depletion length increases, and hence the concentration gradient ∇c and resulting diffusive flux decrease [23].

Note that if a battery electrode stores charge by electrochemical intercalation, then the solid-state diffusion of ions within the electrode structure is an important mass transfer process that must also be considered. In the case where diffusion in the solid is completely rate-limiting, the ion concentration within the electrolyte will be equal to its bulk concentration everywhere as ion transport is "fast" in the electrolyte (an electrical double layer will still exist very close to the electrode surface). However, the current associated with the electrochemical intercalation of ions will be diffusion-limited as a concentration gradient ∇c develops within the solid electrode, rather than within the electrolyte. As potential is swept further beyond the peak current, ions continue to intercalate and the concentration difference between the intercalation surface sites and the bulk solid decreases, thereby decreasing the concentration gradient and hence the diffusive flux. A typical CV curve shape for faradaic charge storage is presented in Fig. 4B, showing a lithium-ion battery with a $LiFePO_4$/C composite cathode, which stores charge by electrochemically intercalating Li^+ ions [24].

Pseudocapacitive voltammograms show both characteristics of capacitive and faradaic diffusion-limited charge storage. The CV curve shape of a pseudocapacitive material often has a generally rectangular-like shape while showing less pronounced current waves. Pseudocapacitive materials operate in a regime that is either (i) not strongly mass transfer- or reaction-limited ($Da_{el} \sim 1) Da_{el} \sim 1$) or (ii) completely reaction-limited, where mass transport is negligible ($Da_{el} \ll 1$), depending on the system and scan rate. Unlike in a faradaic diffusion-limited system, the pseudocapacitive system does not enter a strongly diffusion-limited regime: the concentration of electroactive species at the electrode surface is never completely depleted, resulting in a current that does not increase or decrease precipitously and thus the rectangular-like CV curve shape [23]. For example, the CV scan of a δ-MnO_2 electrode in 1 mol L^{-1} $NaSO_4$ [25] shows a typical pseudocapacitive voltammogram shape (Fig. 4C).

Note that the CV or LSV experimental conditions need to be chosen carefully and the shape alone cannot give a conclusive statement about the system's charge storage mechanism. If the scan rate is fast compared to the apparent rate of the faradaic redox reaction, r_{rxn}^{app}, then the electrochemical reaction will not have time to occur and any current will be dominated by any true capacitive charge storage [2,3]. Similarly, when "slow" surface reactions are present, redox reactions are best identified using slow scan rates (usually <1-10 mV s^{-1}) as the electrochemical reaction must occur during the time over which the potential is swept.

4.1.2. Quantitative analysis of variable-rate voltammograms

Quantitative analysis of a variable-rate CV enables charge storage processes to be distinguished in hybrid systems by measuring how the current i scales with the scan rate υ, as previously suggested by Conway [4]. If the electrochemical reaction is faradaic and completely diffusion-limited ($Da_{el} \gg 1$), then $i \sim \upsilon^{0.5} i \sim \upsilon^{0.5}$. If the electrochemical reaction is completely non-diffusion-limited ($Da_{el} \ll 1$) and thus capacitive and/or pseudocapacitive, then $i \sim \upsilon i \sim \upsilon$. Despite the fact that

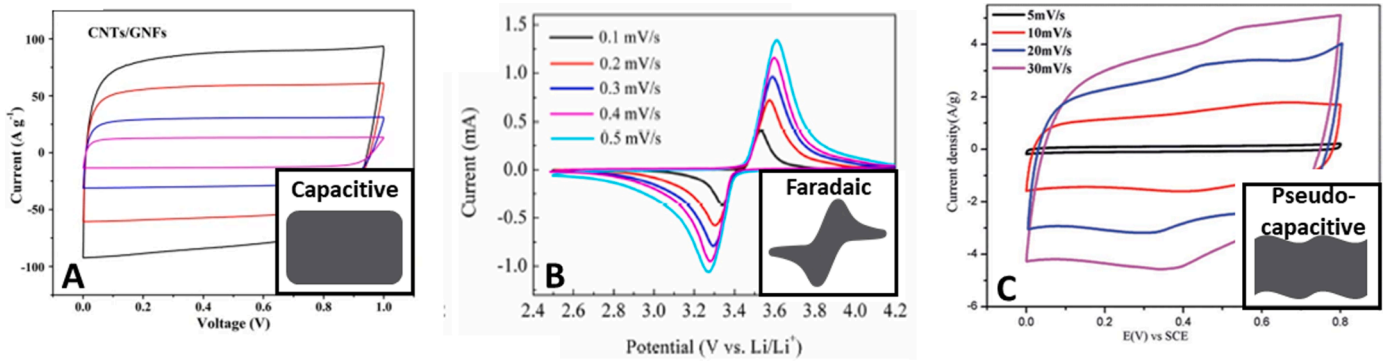

Fig. 4. Representative CV curve shapes for (A) capacitive (Reproduced under the terms of the Creative Commons CC BY license by permission of Nature [21]), (B) faradaic diffusion-limited (Reproduced under the terms of the Creative Commons CC BY license by permission of MDPI [24]) and (C) faradaic non-diffusion-limited (pseudocapacitive) (Reproduced under the terms of the Creative Commons Attribution-Non Commercial 3.0 Unported Licence by permission of The Royal Society of Chemistry [25]) charge storage. Insets in (A, B and C) show schematic shape of cyclic voltammograms for capacitive (box shape), faradaic (peak shapes) and pseudocapacitive (box shape with current waves) charge storage.

pseudocapacitive charge storage is faradaic in nature, its rate-dependency is identical to that of capacitive charge storage, so they cannot be distinguished by scaling relationships alone. Nevertheless, after we discuss methods to distinguish between faradaic diffusion-limited and (pseudo)capacitive charge storage, we explain below a simple method to further disentangle pseudocapacitive and (true) capacitive contributions. Note that if an electrochemical process is not reversible, then instead of CV scans, multiple LSV scans can be performed at different rates, each on a pristine system.

'Lindström's Method' (Power-law method): The treatment by Lindström et al. [26] provides an indication of the different charge storage contributions present in the electrochemical system. Here, the current is assumed to vary with the scan rate according to a power law,

$$i(v) = av^b \quad (12)$$

where a and b are constants. The data are plotted as log(i) *vs.* log(v), yielding a linear relationship with the slope b. If the slope b (or power law 'b-value') is 0.5, the system shows faradaic diffusion-limited behavior. On the other hand, if b-value is 1, pure non-diffusion-limited (capacitive and/or pseudocapacitive) behavior is observed [8,26–28]. A b-value between 0.5 and 1 indicates a mixed regime where the current is controlled by both diffusion and the rate of electrochemical reaction. A step-by-step guide for the determination of the b-value is given in the Supplementary Information, SI 1.

'Dunn's Method': A more quantitatively rigorous approach, enabling the relative proportions of each charge storage process to be disentangled, can be performed by using 'Dunn's method' [8]. This approach assumes that the current can be separated into faradaic diffusion-limited and (pseudo)capacitive non-diffusion-limited contributions using the scaling relationships discussed above: the non-diffusion-limited current scales linearly with the scan rate ($i \sim vi \sim v$) while the diffusion-limited current scales like the square-root of the scan rate ($i \sim v^{0.5} i \sim v^{0.5}$), whose contributions are assumed to be additive:

$$i(v) = av + bv^{0.5} \quad (13)$$

A plot of $i/v^{0.5}$ *vs.* $v^{0.5}$ provides the slope a and intercept b, which reveals the (pseudo)capacitive non-diffusion-limited and faradaic diffusion-limited contributions to the current, respectively, at every measured potential of the CV scan [8,27,29–31].

Note that the total capacity Q stored over any potential sweep can be determined by integrating the current over time throughout the entire scan, or $Q = \int i\, dt$. Thus, the overall capacity contributions due to faradaic diffusion-limited current, Q_{farad}, and (pseudo)capacitive current, Q_{cap}, can be calculated by integrating their respective current contributions ($i_{farad}(v) = bv^{0.5}$ and $i_{cap}(v) = av$) over time, where a and b are determined using Eq. (13). The quantities Q_{farad}/Q and Q_{cap}/Q are the fractions (or percentages, if desired) of charge stored due to faradaic and (pseudo)capacitive processes over the specified potential window ΔE and scan rate v, respectively, which yield insights into how mass transfer of the electroactive species affects (and/or limits) the current for a given system and set of experimental conditions.

Disentangling Pseudocapacitive and True Capacitive Charge Storage: Pseudocapacitive and true capacitive charge storage contributions can be further distinguished quantitatively, as Q_{cap} includes charge stored due to both pseudocapacitive faradaic reactions, Q_{pseudo}, and true capacitive storage due to electrical double layer charging, Q_{DL}, which are additive: $Q_{cap} = Q_{pseudo} + Q_{DL}$. To distinguish between them, it is first necessary to determine a potential window ΔE^*, far from any redox peaks due to faradaic reactions, where the current scales linearly with the scan rate ($i \sim v$). The electrical double layer capacitance C_{DL}, which is a constant for any system, can then be determined by applying a relationship analogous to Eq. (10), $\Delta Q^*_{DL} = C_{DL}\Delta E^*$, where $\Delta Q^*_{DL} = i\Delta t$ over the time corresponding to this potential region. Once C_{DL} is known, the total double layer capacity Q_{DL} that accounts for the stored charge over the entire potential window ΔE can then be calculated according to Eq. (10), or $Q_{DL} = C_{DL}\Delta E$. The quantities Q_{pseudo}/Q and Q_{DL}/Q are the fractions (or percentages, if desired) of charge stored due to pseudocapacitance and true (electric double layer) capacitance, respectively, over the specified potential window ΔE and scan rate v.

Step-by-step guides for how to determine the power law b-value by the 'Lindström' method (Eq. (12)) and disentangle the (pseudo)capacitive and faradaic charge storage contributions by the 'Dunn' method (Eq. (13)) are given in the Supplementary Information, SI 1 and SI 2, respectively. In addition, we provide both a MATLAB GUI and a JavaScript code to disentangle faradaic and (pseudo)capacitive contributions from variable-rate CV data. Furthermore, a step-by-step guide for disentangling pseudocapacitive and capacitive charge storage contributions is provided in the Supplementary Information, SI 3. The application of these methods to disentangle faradaic, pseudocapacitive, and capacitive charge storage contributions in a rechargeable battery is shown in Example 1.

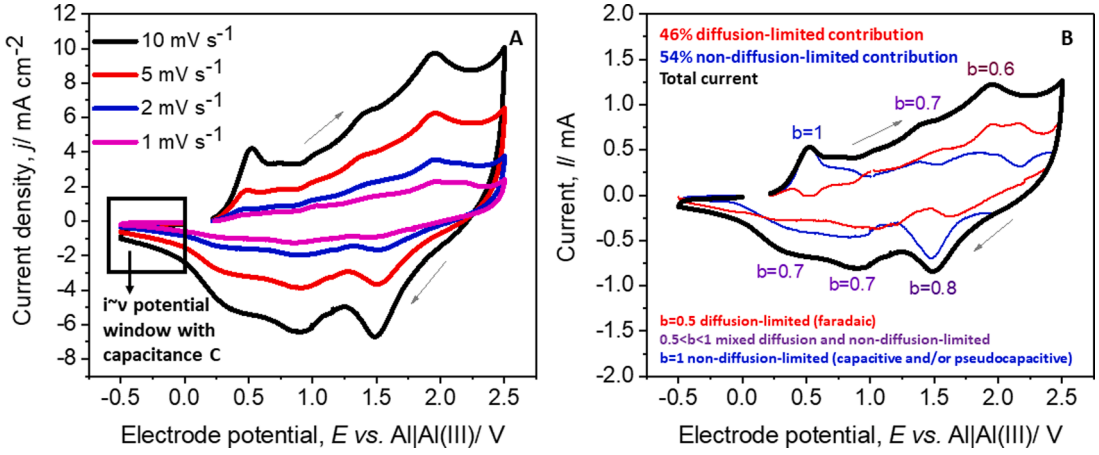

Fig. 5. (A) Variable-rate CV curves of PEDOT in a rechargeable aluminum metal battery using a chloroaluminate EMImCl-$AlCl_3$ electrolyte. (B) Extraction of diffusion-limited (red) and non-diffusion-limited (blue) charge storage contributions (Eq. (13)) as well as power law b-values (Eq. (12)) for the 10 mV s^{-1} scan [8,26]. (Unpublished data obtained by R.J. Messinger group at CCNY).

Example 1

Faradaic, pseudocapacitive, and capacitive charge storage contributions are quantitatively disentangled (Supplementary Information, SI 2) in a rechargeable aluminum metal battery using a conductive polymer (electropolymerized PEDOT) as the positive electrode material in a chloroaluminate ionic liquid electrolyte (Fig. 5). The CV scan rate was varied between 1 and 10 mV s^{-1} such that peak shifts with respect to potential remained negligible (Fig. 5A). Using Dunn's method (Eq. 13), the overall faradaic diffusion-limited and (pseudo)capacitive charge storage contributions were 46% (Q_{farad}/Q, red) and 54% (Q_{pseudo}/Q, blue) at 10 mV s^{-1}, where their specific ratios vary with potential (Fig. 5B). Moreover, the power law *b*-values determined by the Lindström method (Eq. (12)) at selected potentials correspond well with their relative contributions. The variable-rate CV analyses suggests that chloroaluminate anions charge compensate first at the polymer surfaces during charge (oxidation), causing a significant pseudocapacitive current. The faradaic current becomes increasingly diffusion-limited as the anions insert into the polymer, a process that correlates with a notable swelling of the micro-structure of the polymer [32]. To extract the true capacitive contribution, a potential window ΔE^* far from the redox peaks where $i \sim \upsilon$ (here, -0.5 V to 0 V) was used to determine the electrical double layer capacitance C_{DL} (Supplementary Information, SI 3), which was 0.04 mF. Using this value, the capacity associated with electric double layer charging Q_{DL} accounts for only for 0.1% of the total capacity *Q*.

4.2. Potential step methods (chronocoulometry and chronoamperometry)

Potential step methods are also powerful tools to extract (pseudo) capacitive and faradaic contributions, including values for the electrical double-layer capacitance Q_{DL} and pseudocapacitive contributions that originate from ion adsorption processes. In a single potential step experiment, the current response is recorded as a function of time immediately after the potential step. If the electrochemical reaction is reaction-limited over the experimental conditions ($Da_{el} \ll 1$), the current *i vs. t* decays exponentially over a very short time (typically, on the order of milliseconds). If the electrode is exposed to a sufficiently high potential (typically, 200 to 300 mV over the standard potential), the electroactive species is consumed quickly at the electrode surface and a concentration gradient is produced, resulting in a diffusive flux. For diffusion-limited charge storage ($Da_{el} \gg 1$), the current follows the Cottrell equation [2,23]

$$i(t) = \frac{z_e F A D^{0.5} c_0}{\pi^{0.5} t^{0.5}} \tag{14}$$

where *A* is the electrode surface area, *D* is the ion diffusion coefficient, c_0 is the concentration of electroactive ions in the bulk electrolyte, and *t* is the time of the current response after the potential step [2]. Note that this equation is best applied when concentration gradients develop within the electrolyte (e.g., during metal electrodeposition) as opposed to the electrode (e.g., during electrochemical ion intercalation, when ion diffusion within the solid is rate limiting).

The total capacity *Q* from the potential step experiment, determined by integrating the current with respect to time, can be written as

$$Q = \underbrace{\frac{2 z_e F A D^{0.5} c_0 t^{0.5}}{\pi^{0.5}}}_{\text{diffusion-limited}} + \underbrace{Q_{DL} + z_e F A \Gamma}_{\text{non-diffusion-limited}} \tag{15}$$

The first term describes the faradaic diffusion-limited contribution (Q_{farad} for a potential step experiment) based on the Cottrell relationship (Eq. (14)). The second term, Q_{DL}, describes the true capacitive contribution associated with electric double layer charging. The third term, $z_e F A \Gamma$, is attributed to any capacity that arises from pseudocapacitive adsorption processes on the electrode surface (Q_{pseudo}), where Γ is the surface concentration with dimensions of mol per unit area. Note that this term can be generalized to include other pseudocapacitive processes, if desired. The second and third terms of Eq. (15) represent the overall (pseudo)capacitive charge storage contribution Q_{cap} (Eq. (16)).

$$Q_{cap} = z_e F A \Gamma + Q_{DL} \tag{16}$$

To separate capacitive from faradaic diffusion-limited charge storage contribution by potential step experiments, the total capacity *Q* Eq. (15)) can be represented by plotting *Q vs.* $t^{0.5}$, also known as an Anson plot. Doing so yields a linear relationship for capacity due to diffusion-limited current, while the *y*-axis intercept reflects all (pseudo)capacitive contributions Q_{cap} (Eq. (16)) [2]. A step-by-step guide is given in the Supplementary Information, SI 4.

4.2.1. Ion diffusion coefficients

At this point, we highlight that ion diffusion coefficients can be calculated based on the Cottrell relationship, but this assumes that the current is completely diffusion-limited ($Da_{el} \gg 1$). Notably, this assumption applies also to diffusion coefficients determined by the well-known Randles–Ševčík equation, which is based upon the Cottrell relationship. Thus, if an electrochemical system has appreciable (pseudo)capacitive contributions, these relationships cannot be used to compute ion diffusion coefficients, which unfortunately is sometimes done in the literature. The diffusion coefficient can be estimated taking into account mixed (diffusion-limited and non-diffusion-limited) mass transport by using EIS (as described by Xu et al. [33]). Remember, the determined diffusion coefficient in such cases, particularly for heterogeneous and/or porous electrodes with appreciable (pseudo)capacitive contributions, is a global "average" value that may represent multiple ion diffusion processes (e.g., in the electrolyte phase in the porous electrode and/or in the solid-state) if one process is not strongly rate-limiting. Furthermore, potentiostatic or galvanostatic intermittent titration (PITT and GITT, respectively) methods are often used to determine diffusion coefficients especially for battery intercalation electrodes as described by Levi et al. [34]. Again, for the PITT and GITT methods, it is important to understand the different charge storage contributions of the system so that true and pseudo-Cottrellian domains in the chronoamperometric curves can be determined, using for example Fickian diffusion and moving boundary models. Further explanations regarding the moving boundary model are provided by Shin et al. [35, 36]. Diffusion coefficients are computed, in all cases, using models that assume pure diffusion limitations, so care must be taken to ensure that the correct experimental conditions, data, and model are used.

4.3. Qualitative interpretation of galvanostatic charge/discharge curves

Electrochemical energy storage devices are often characterized by galvanostatic (constant current) charge/discharge cycling to determine specific energy and power, as well as rate capability, capacity retention, and cycle life. Similar to the shape of a CV or LSV curve, galvanostatic charge/discharge curves can suggest the primary charge storage mechanism (Fig. 6). The data is usually plotted as potential *vs.* time, capacity, or specific capacity.

Capacitors and some pseudocapacitors show triangular charge/discharge curves following a linear increase/decline in potential with the state-of-charge. High-surface-area carbon materials, such as activated carbon, graphene, and carbon nanotubes are commonly used as capacitive electrodes. Capacitive carbon electrodes derived from natural

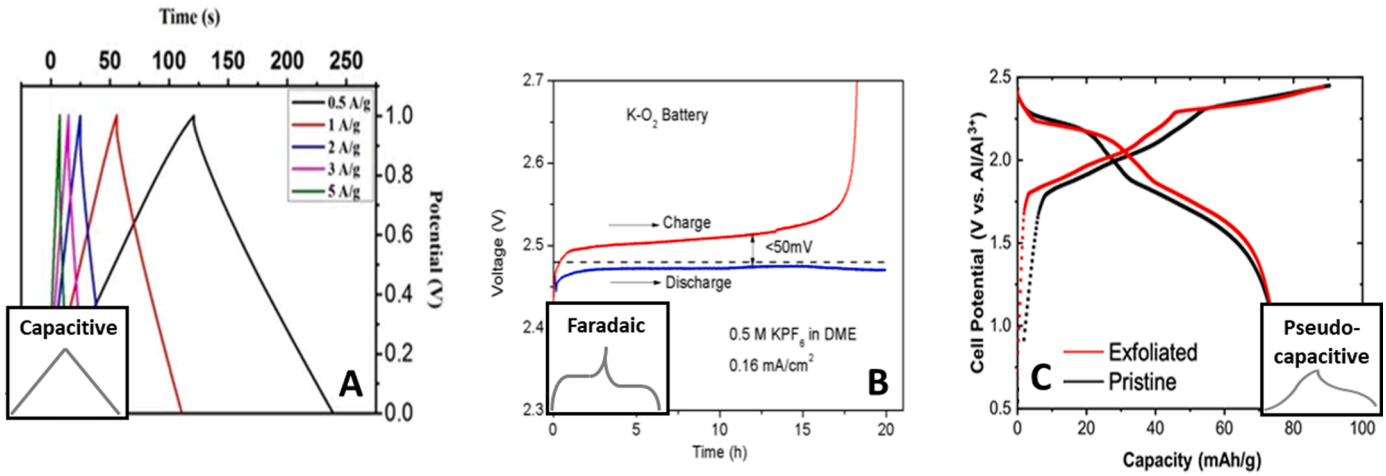

Fig. 6. Representative galvanostatic charge/discharge curve shapes for (A) capacitive (Reproduced under the terms of the Creative Commons CC BY license by permission of Nature [37]), (B) faradaic diffusion-limited (Reproduced by permission of the American Chemical Society [40]) and (C) pseudocapacitive charge storage (Reproduced under the terms of the Creative Commons Attribution 4.0 License by permission of The Electrochemical Society [33]).

materials [37–39] are a current trend. For example, KOH-activated banana stem carbon in aqueous 6 M KOH (Fig. 6A) [37] shows a typical galvanostatic capacitive charging/discharging behavior.

Systems storing energy by faradaic charge storage will show one or more galvanostatic charge/discharge plateaus at the potentials associated with the electrochemical redox reactions. The drop or rapid increase of the potential indicates the end of charge or discharge, respectively. For example, a K-O_2 battery with 0.5 M KPF_6 in DME shows distinct charge/discharge plateaus related to the faradaic diffusion-limited one-electron redox process of O_2/O_2^- and formation of KO_2 with K^+ ions (Fig. 6B)[40].

Systems with mixed (pseudo)capacitive and faradaic charge storage contributions can either have sloping charge/discharge curves or triangular-like shapes with implications of potential plateaus, depending on their relative contributions. For example, an aluminum-graphite battery with chloroaluminate ionic liquid electrolyte has significant pseudocapacitive charge storage character due to the "fast" electrochemical intercalation of chloroaluminate anions into graphite, which is qualitatively reflected by the sloping charge/discharge curves that do not have either well-defined constant potential plateaus or perfect triangular-like shapes (Fig. 6C) [33]. The shape of the charge/discharge curves can also be altered by the particle size of an electroactive material, influencing pseudocapacitive contributions, as shown below [2,5, 10].

4.4. *Electrochemical impedance spectroscopy*

EIS is an advanced method to quantitatively distinguish between capacitive and faradaic charge storage. The frequency variation of an applied alternating current (AC) signal on the energy storage system can reveal different electrochemical phenomena based on their frequency response. A three-electrode setup is necessary to isolate single-electrode processes, as a two-electrode set-up will show impedances from both electrodes.

An impedance spectrum can be separated into three parts: the low (commonly for intercalation materials: ≤10 mHz), medium (10 mHz-1 kHz) and high (≥1 kHz) frequency range. The low frequency range reveals phenomena such as mass transport in the solid-state (e.g., ion diffusion within an intercalation electrode). The medium frequency range typically reveals processes at the electrode-electrolyte interface (e.g., charge transfer reactions and electrical double layer charging). The high frequency range includes cell resistances (e.g., electrolyte and interfacial resistances).

Impedance spectra can be represented as complex plane plots, commonly known as Nyquist plots, or Bode plots. Nyquist plots show the real part of the impedance, Z_{RE}, *vs.* the imaginary part, $-Z_{Im}$, and reveal individual phenomena easily. The Bode plots are represented as the logarithm of the overall impedance log*(Z)* *vs.* the logarithm of the frequency log*(f)* or phase angle φ *vs.* log*(f)* and therefore show characteristic changes of these parameters as a function of the frequency. Because the frequency is not obvious in the Nyquist plots and small impedances may be obscured by large impedances, it is always useful to represent both Nyquist and Bode plots of the same data set.

Physical phenomena occurring at the working electrode (3-electrode set up) or the energy storage device (2-electrode set up) may be modeled by electric circuit elements, such as resistors, capacitors, inductors, and elements approximating diffusion processes (e.g., Warburg-element for semi-infinite diffusion and M-element for modified restricted diffusion), which model different physical processes of the system. These circuit elements can describe phenomena such as internal resistances, electrical double layer charging, and ion transport phenomena. The resulting circuits offer mathematical expressions for how the electrical impedance varies with frequency, which can be used to fit the experimental data by varying parameter models [9].

To understand how to distinguish capacitive and faradaic contributions by modeling EIS data, two types of simple resistor-capacitor element (RC-elements) connections must be considered. For example, the simplest way to model a faradaic diffusion-limited charge transfer process is by a parallel RC-circuit; here, the resistor represents the charge transfer resistance R_{ct} associated with the faradaic reaction and the capacitor represents electrical double layer charging with capacitance C_{DL} (which occurs at every electrolyte-electrode interface, even if small). On the other hand, non-diffusion-limited (pseudo)capacitive charge storage can be modeled by a serial RC-circuit with a "capacitance" C_P (or constant phase element, see below) in conjunction with a charge transfer resistance R_{ct}. The transition from a series towards a parallel RC-circuit is illustrated below in Example 2, where an electrode's faradaic charge storage becomes increasing diffusion-limited as its state-of-charge increases.

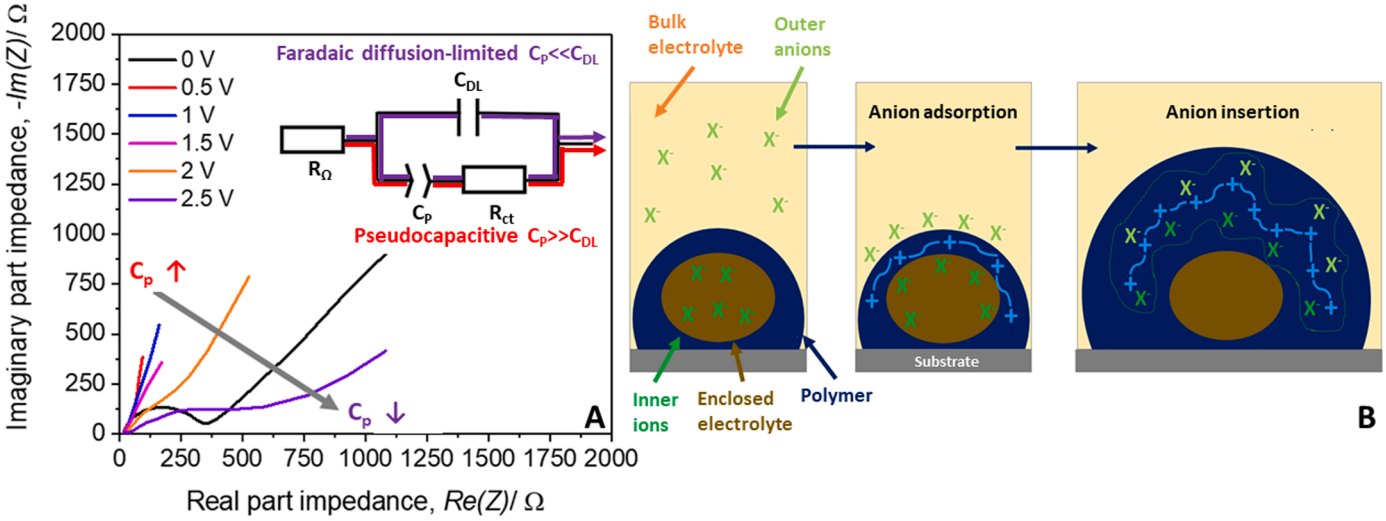

Fig. 7. (A) EIS Nyquist plot of PEDOT in a rechargeable aluminum metal battery using a chloroaluminate EMImCl-$AlCl_3$ electrolyte at different states-of-charge. Inset: model circuit. (B) Schematic illustration of the charging process of a conductive polymer grain. (Unpublished data obtained by R.J. Messinger group at CCNY).

Example 2

EIS data for the same polymer-ionic liquid system presented in Example 1 and Fig. 5 will be modeled with an equivalent circuit (Fig. 7A, inset), whose elements can distinguish between faradaic diffusion-limited and pseudocapacitive contributions that furthermore vary with state-of-charge. A simple model circuit includes the inner cell resistance R_Ω, the polymer electrode resistance R_{ct}, the electric double layer capacitance C_{DL} and another capacitor C_P that describes pseudocapacitive charge storage contributions. The Nyquist plot (Fig. 7A) shows steep sloped curves when the polymer is at low states-of-charge (0.5 V to 1.5 V), which suggest a dominant pseudocapacitive process. At higher-state of-charges (2 V to 2.5 V), the faradaic diffusion-limited contribution becomes dominant as manifested by the formation of a semi-circle. At lower states-of-charge, the faradaic reaction shows a lack of significant diffusion-limitations, which is due to the fast adsorption and accumulation of charge-compensating anions at the polymer surface (pseudocapacitive effect, C_P) (Fig. 7B). Thus, the equivalent circuit can be represented by a series connection where the current passes through R_{ct} and C_P. Because $C_P \gg C_{DL}$, the C_{DL} circuit element is negligible. At higher states-of-charge, the faradaic reaction becomes increasingly diffusion-limited associated with the oxidation of the polymer and slow diffusion of anions into the polymer structure (Fig. 7B). The related equivalent circuit changes to a parallel configuration where the overall current must pass the RC element including the electrical double layer capacitance C_{DL} because now $C_P \ll C_{DL}$ [9].

However, the shape of the impedance curve, similar to the shape of a CV curve or a charge/discharge curve, can provide only an indication of the charge storage mechanism. In particular, pseudocapacitive effects can also be represented in a semi-circle since the underlying charge storage mechanism is faradaic; a pseudocapacitive semi-circle typically appears in the mid-frequency region and has a characteristic diameter that represents the charge transfer resistance R_{ct}. The charge transfer resistance is usually lower for faradaic reactions that are pseudocapacitive (smaller semi-circle diameter).

In addition, the semi-circle might be distorted, where the impedance can be modeled by constant phase element (CPE) with a depression factor α ($-1 \leq \alpha \leq 1$), according to

$$Z_{CPE} = \frac{1}{C(j\omega)^{\alpha}} \text{ with } \omega = 2\pi f \tag{17}$$

The depression factor can be modeled (Eq. (17)) by using a constant phase element (CPE) that represents a (pseudo)capacitive layer which is imperfect and has inhomogeneities (e.g., porous surfaces) [9]. The depression factor also decreases with geometric irregularities of the capacitive layer, which is linked to energetic phenomena such as the dispersion of frequency due to surface disorder [41].

The phase angle φ (Eq. (18)) is an indicator of diffusion limitations, especially in the low frequency region. A low-frequency phase angle of 45° usually indicates to diffusion-limited ion transport. A low-frequency phase angle of 90°, on the other hand, represents ideal capacitive behavior with no diffusion limitations. A low-frequency phase angle of 0° describes complete resistive behavior.

$$\tan(\varphi) = \frac{-Z_{Im}}{Z_{Re}} \tag{18}$$

Taberna et al. [42] proposed a method to distinguish between faradaic diffusion-limited and (pseudo)capacitive charge storage by

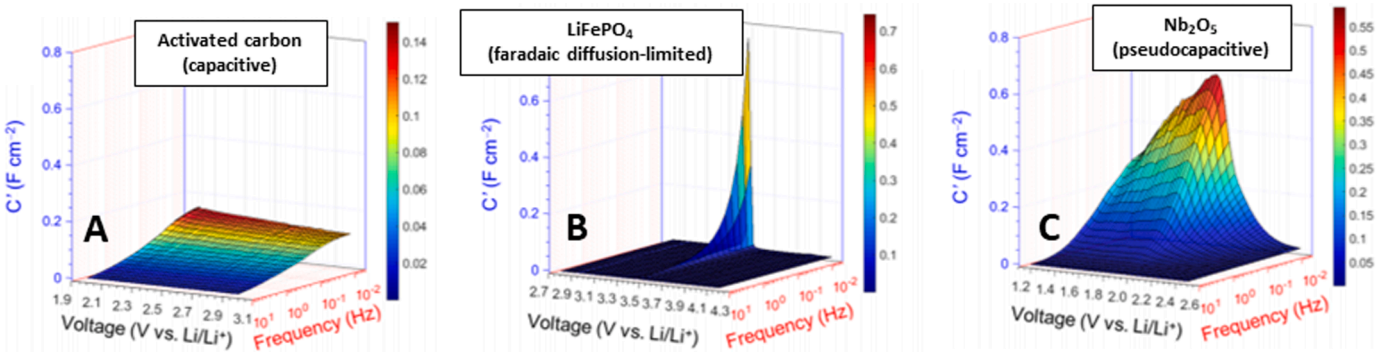

Fig. 8. 3D Bode plots of the 'real capacitance *C*' (qualitative measure of pseudocapacitance) as a function of the frequency at different potentials of (A) activated carbon YP50F (capacitive), (B) $LiFePO_4$ (faradaic diffusion-limited) and (C) Nb_2O_5 (pseudocapacitive). (Reproduced and adapted by permission of The American Chemical Society [43]).

impedance spectroscopy, which was later used by Ko et al. [43]. The method defines a capacitance *C*' (real part; authors define as 'real capacitance') and *C*'' (imaginary part), according to

$$C' = \frac{-Z_{Im}(\omega)}{\omega|Z(\omega)|^2} \tag{19}$$

$$C' = \frac{Z_{RE}(\omega)}{\omega|Z(\omega)|^2} \tag{20}$$

Often, *C*' is defined as a 'capacitance' that describes faradaic charge storage, though its physically meaningful value as a 'capacitance' is not well-defined, as the underlying charge storage mechanism is faradaic (see "C_{pseudo}" discussion above). Instead, *C*' is a value that correlates with the pseudocapacitive character of the system. *C*'' refers to the capacitance that arises from true capacitive charge storage (C_{DL}).

The 3D Bode-type plots with potential as an additional axis (Fig. 8) represent *C*' for materials with predominantly capacitive (activated carbon; Fig. 8A), faradaic diffusion-limited ($LiFePO_4$, Fig. 8B) and pseudocapacitive (Nb_2O_5, Fig. 8C) charge storage contributions that furthermore vary depending on the state-of-charge [43]. For the activated carbon, *C*' remains small in magnitude and approximately constant over the investigated potential window and frequency range, consistent with electrical double layer charging. The $LiFePO_4$ battery electrode shows a peak in *C*' at 3.5 V, where the electrochemical intercalation of Li cations occurs, suggesting that Li-ion intercalation in $FePO_4$ may have some pseudocapacitive character. Nb_2O_5, on the other hand, shows a high value for *C*' over the whole measured potential window as Li-ion intercalation into the structure is pseudocapacitive [44], with a maximum near the potential associated with the Li-ion intercalation reaction (See Fig. 8).

5. Electrochemical energy storage systems with mixed charge storage mechanisms

Energy storage systems today may blend materials with faradaic, pseudocapacitive and capacitive charge storage mechanisms into one electrode, or pair electrodes with different dominant charge storage mechanisms into one device. Here, by "pseudocapacitive charge storage mechanism," we indicate that the fundamental physical nature of the charge storage is indeed faradaic in nature, but whose overall rate of electrochemical reaction is either non-diffusion-limited ($Da_{el} \ll 1$) or in a mixed transport regime ($Da_{el} \sim 1$) over common experimental conditions. In the literature, these systems are often classified as fast-charging batteries, hybrid battery-capacitors, hybrid supercapacitors or asymmetric systems.

First, we define electrodes that blend together different materials and/or structures that store charge according to different primary charge storage mechanisms, which are generally known as *hybrid electrodes*. We define *fast-charging battery electrodes* as electrodes that blend faradaic diffusion-limited and pseudocapacitive charge storage characteristics. *Hybrid battery-capacitor* and *hybrid supercapacitor electrodes* blend faradaic diffusion-limited and capacitive charge storage, where hybrid battery-capacitor electrodes exhibit greater faradaic diffusion-limited charge storage contributions than hybrid supercapacitor electrodes, whose capacitive charge storage contribution is more prominent. Second, we define the device itself based on the electrode pair. Generally, *asymmetric systems* or *hybrid systems* refer to electrical storage devices made of electrodes with different primary charge storage mechanisms. Commonly, asymmetric systems are divided into two categories: systems with pseudocapacitive electrodes paired with faradaic diffusion-limited electrodes, which are called *fast-charging batteries*, and those with a (true) capacitive electrode alongside a faradaic (including pseudocapacitive) electrode, which can be called either a *hybrid supercapacitor or hybrid battery-capacitor*. Several reviews [45–48] were published describing the many aspects of asymmetric systems such as the materials used [49–51], the mechanisms, the formation of 3D porous carbon [52], and more [51,53,54].

Although a mixture of capacitive and faradaic charge storage mechanisms characterizes the electrochemical energy storage systems mentioned above, the device should be identified first and foremost by its primary or most prominent charge storage mechanism. For example, if capacitive charge storage is dominant, the device should be characterized mainly as a capacitor. *Vice versa*, if a faradaic charge storage (diffusion-limited and/or pseudocapacitive) is dominant, the system should be classified as a battery. Correctly distinguishing the different charge storage mechanisms is important, as the concept and quantitative

value of capacitance only make physical sense for truly capacitive charge storage. For capacitors, it is important to measure the specific capacitance (F g^{-1}) so that a normalized comparison between different systems is possible. Note that the current in a capacitive system is commonly described by the specific current (mA g^{-1}). For batteries, a specific capacity (mAh g^{-1}) is usually reported, while currents are often described by either the specific current (mA g^{-1}) or (areal) current density (mA cm^{-2}).

Both capacitors and batteries are characterized by their specific energy E_{spec} and power P_{spec} as well as energy E_{vol} and power P_{vol} density (Eqs. (21)–(24)), which can be calculated using data from galvanostatic discharge experiments according to:

$$E_{spec} = \frac{\int E dQ}{m} \tag{21}$$

$$E_{vol} = \frac{\int E dQ}{V} \tag{22}$$

$$P_{spec} = \frac{EI}{m} \tag{23}$$

$$P_{vol} = \frac{EI}{V} \tag{24}$$

The term "specific" refers to the energy and power per mass (gravimetric, with typical units of Wh kg^{-1} or W kg^{-1}) while the term "density" relates to the energy or power per volume (volumetric, with typical units of Wh L^{-1} or W L^{-1}), respectively. Note that some researchers use the term "gravimetric energy density" to denote the former and "volumetric energy density" to denote the latter.

Hybrid electrochemical energy storage systems can be analyzed using the methods and framework above to quantitatively distinguish their charge storage mechanisms as well as define the primary mechanism and thus the system (e.g., battery, supercapacitor). As discussed above, all energy storage devices have a charge capacity that describes the quantity of stored charge Q due to a current I over a period of time t, $Q = \int i\, dt$ [1] during an electrochemical experiment. The total capacity Q is composed of both (pseudo)capacitive and faradaic contributions, $Q = Q_{cap} + Q_{farad}$, while Q_{cap} can be further separated into $Q_{cap} = Q_{pseudo} + Q_{DL}$ due to pseudocapacitive and double layer charging contributions; their relative ratios define the system. For example, the exfoliated graphite electrode in an aluminum-graphite battery from Xu et al. [33], which stores charge by electrochemically intercalating chloroaluminate anions, was characterized by variable-rate CV. The sweep at 3 mV s^{-1} resulted in a total capacity Q of 417 mAs, where Q_{farad} was 71 mAs and Q_{cap} was 346 mAs (Eq. (13)). The capacitance C_{DL} was calculated to be of 10 mF (or 10 F g^{-1}), which resulted in a Q_{DL} of 28 mAs and therefore a Q_{pseudo} of 318 mAs. Based on their relative contributions, Q_{farad}, Q_{pseudo}, and Q_{DL} were 17%, 76%, and 7% of the total capacity. Therefore, this electrochemical energy storage system can be classified as a battery, specifically a fast-charging battery. The authors revealed that gentle exfoliation enhanced the pseudocapacitive intercalation of chloroaluminate anions into graphite, while preserving specific energy, due to a combination of reduced electrode tortuosity, increased accessibility of interstitial pores to $AlCl_4^-$ ions, and fewer blocked edge sites, all of which enhances ion mass transport within the porous electrode structure.

In the following, we provide selected examples of mixed electrochemical energy storage systems that use hybrid electrodes that blend different combinations of charge storage mechanisms: (i) faradaic diffusion-limited and pseudocapacitive, (ii) faradaic diffusion-limited and (true) capacitive, and (iii) pseudocapacitive and (true) capacitive.

5.1. Electrodes blending faradaic diffusion-limited and pseudocapacitive charge storage

Fast-charging battery electrodes blend faradaic diffusion-limited and pseudocapacitive charge storage characteristics (over common experimental conditions) to enhance the specific power of the device. Their high rate capabilities stem from significant pseudocapacitive contributions, which can be enhanced by the following strategies: (i) controlling the electrode structure to decrease ion diffusion lengths within the solid electrode and/or electrolyte within the porous electrode, or to increase electroactive surface area (e.g., by hierarchically structuring the electrode, decreasing electroactive particle size, reducing tortuosity, etc.), (ii) for battery intercalation electrodes, using electrode materials where the inherent diffusivity of the ions within the solid framework structure is sufficiently high (note that phase changes induced upon ion intercalation slow mass transfer considerably), or (iii) blending multiple electroactive materials, with different ion transport and energy storage properties, together in a composite electrode. Both strategies, at their core, involve enhancing rates of ion mass transport and thus reducing the electrochemical Damköhler number, Da_{el}, associated with rate-limiting kinetic and mass transfer processes. Note that multiple strategies can be employed simultaneously.

Example fast-charging battery electrodes include Nb_2O_5 [44] or nano-sized titania [8,26,55,56] anodes for Li-ion batteries, which offer significant pseudocapacitive charge storage due to "fast" solid-state Li^+ diffusion or increased surface area for electrochemical adsorption of Li^+ cations, respectively. Similarly, in aluminum batteries, conductive polymers [32] store charge pseudocapacitively due to the fast initial adsorption and diffusion of chloroaluminate anions, while exfoliated graphite electrodes [33] do so because of the inherently fast solid-state diffusion of chloroaluminate anions within graphite coupled with structural modifications upon exfoliation that reduce ion diffusion lengths [28,33]. Both examples are highlighted above.

For example, researchers have controlled electrode structure to enhance pseudocapacitive charge storage in Li-ion batteries. Lindström et al. [26] studied nanoporous titania electrodes for Li-ion batteries, where the individual contributions of volume and surface processes in TiO_2 were analyzed for the first time. Strong pseudocapacitive effects were observed in the nanoporous TiO_2 electrodes, which the authors attributed to the electrochemical adsorption of Li^+ ions on the TiO_2 surfaces [26]. These early studies were confirmed later by Kavan et al. [55], followed by Wang et al. [8] and Brezezinski et al. [56] who studied the effect of active surface area and particle size on the pseudocapacitive charge storage in TiO_2 nanoparticles (see Example 3 below). Similarly, Okubo et al. [57] first observed the effects of reducing particle size on the charge/discharge performance of $LiCoO_2$ electrodes, finding that nanocrystalline $LiCoO_2$ with an average size of 17 nm displayed improved rate capabilities. The contributions of surface charge storage of Li-ion to the total capacity of $LiMn_2O_4$ spinel structures have been studied by Lesel et al. [58,59], where a significant surface charge contribution (>50 %) was observed for particle diameters less than 70 nm [58]. Note that in these examples, pseudocapacitance due to ion adsorption enhanced the rate capabilities (and thus specific power), but there is a tradeoff: the capacity due to electrochemical adsorption may occur at lower potentials compared to electrochemical intercalation, thereby decreasing the specific energy. Also, the charge storage mechanisms are faradaic in nature and the systems above are therefore classified primarily as batteries.

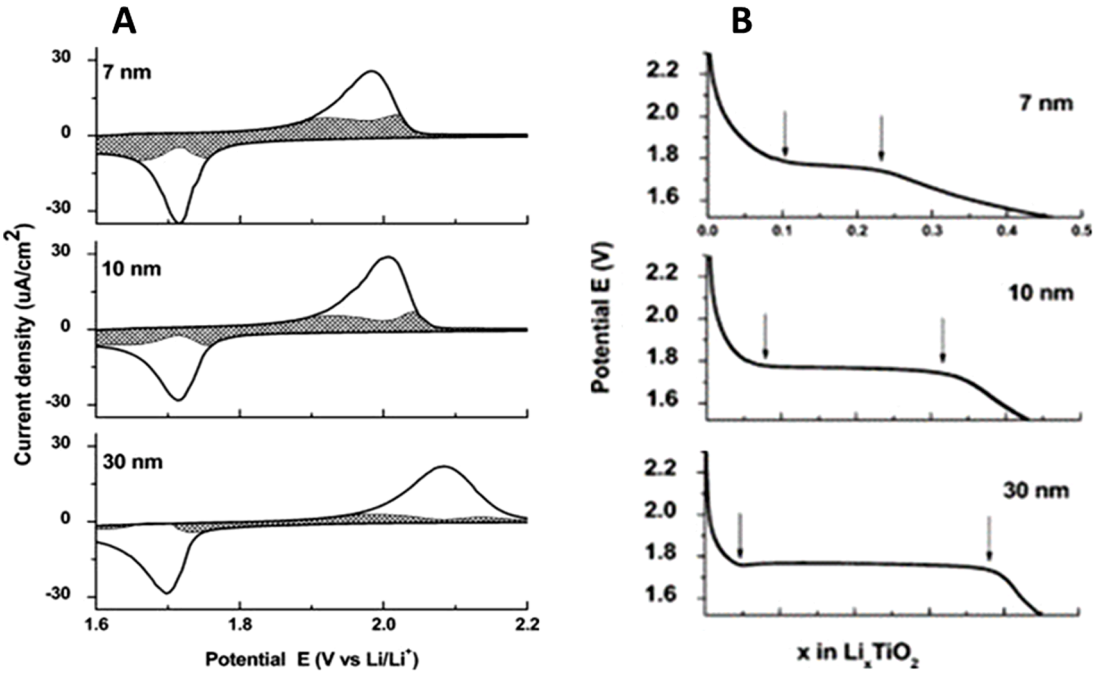

Fig. 9. (A) CV curves of TiO_2 electrodes in Li-ion battery systems prepared with different particle sizes. The pseudocapacitive contributions to the current (shaded areas) were determined by quantitative analyses of variable-rate CV curves and treatment with Eq. (13), revealing enhanced pseudocapacitive current with decreasing particle size. (B) Galvanostatic discharge curves for TiO_2 electrodes at a rate of ~1 C. Reproduced by permission of The American Chemical Society [8].

Example 3

TiO_2 electrodes prepared with varying particle sizes at the nanoscale exhibit varying extents of pseudocapacitive charge storage in Li-ion battery systems, as shown by Wang et al. [8]. Quantitative analyses of CV scans (Fig. 9A, black) reveal that decreasing particle size correlates with increasing pseudocapacitive contributions to the current (shaded area of the CV curve), as determined by Eq. (13) (see Section 4.1 above). Galvanostatic discharge curves (Fig. 9B) show that the well-defined discharge plateau due to electrochemical Li-ion intercalation becomes more sloping as the particle size decreases, qualitatively indicating enhanced pseudocapacitance (see Section 4.3. above). The TiO_2 electrode with the smallest particle size has the highest specific surface area, which increases the (non-diffusion-limited) pseudocapacitive current due to the electrochemical adsorption of Li^+ ions on the TiO_2 surfaces.

5.2. Electrodes blending faradaic diffusion-limited and capacitive charge storage

Hybrid supercapacitor or hybrid battery-capacitor electrodes blend faradaic diffusion-limited and (true) capacitive charge storage. Such electrodes typically combine a redox active material with a high-surface-area carbon material that stores charge by (true) electrical double layer capacitance. The merging of the two mechanisms can increase either the specific energy or power of the system, while typically decreasing the other quantity.

The most common carbon materials for capacitive charge storage in hybrid energy storage systems are sp^2 hybridized carbons. Yet, sp^2 carbon represents a wide range of conductive materials spanning from graphite to graphene and activated carbon to carbon nanotubes. Activated carbon, having a theoretical maximum surface area over 3000 m^2 g^{-1}, is a common capacitive electrode material. It is typically prepared with different pore sizes by a wide variety of methods and from numerous sources [60]. So-called multi-dimensional graphene [61] is also becoming an appealing alternative. The surface area of carbon nanotubes is usually lower than that of activated carbon; however, their electronic conductivity along the nanotube axis is much greater. Single-walled carbon nanotubes (SWCNTs) have a specific surface area of ca. 1600 m^2 g^{-1} and have been shown to have specific capacitances of 100-200 F g^{-1} [62], while vertically grown SWCNTs reached specific capacitances greater than 400 F g^{-1} [63]. The intrinsic flexibility of carbon nanotubes has made them attractive materials for flexible (and wearable) energy storage systems. Graphene has a theoretical specific surface area of 2630 m^2 g^{-1} and specific capacitance of 550 F g^{-1}. Yet, this theoretical capacitance is challenging to reach due to the strong stacking and agglomeration off graphene sheets. Different approaches have been examined to prevent the stacking by introducing various spacers as well as by curving the graphene layers. Furthermore, different treatments of graphene have resulted in 3D graphene-based architectures, such as 3D graphene-based hydrogels, aerogels, foams, and sponges, having very high porosity and surface area [64].

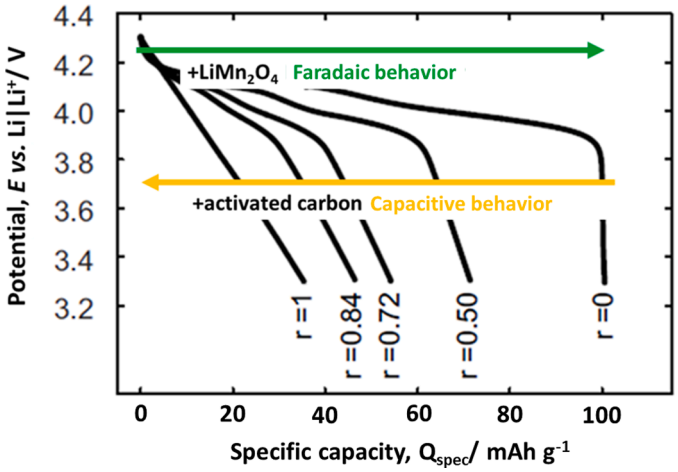

Fig. 10. Galvanostatic discharge curves (C/5 rate) of blended activated carbon-$LiMn_2O_4$ hybrid electrodes with varying mass ratios, *r*, of activated carbon:$LiMn_2O_4$. Reproduced by permission of Elsevier [65].

Example 4

In a hybrid electrode containing different materials that store charge by (true) capacitive and faradaic mechanisms, the primary charge storage mechanism and electrochemical behavior is determined by their relative ratios. For instance, Cericola et al. [65] demonstrated that blending activated carbon (capacitive) and $LiMn_2O_4$ (faradaic) naturally allows the degree of capacitive and faradaic (diffusion-limited) behavior to be tuned (Fig. 10), as reflected in their galvanostatic discharge curves (see Section 4.3 above). Increasing the ratio of activated carbon:$LiMn_2O_4$ resulted in increasing specific power but decreasing specific energy, and *vice versa*. This ratio can furthermore be tuned for a specific energy storage application. For example, a 50:50 mass ratio of both components yields an improved specific capacity of 70 mAh g^{-1} and a higher average discharge potential compared to the activated carbon alone (35 mAh g^{-1}), yet the high specific power associated with activated carbon was maintained [65].

Hybrid capacitive-faradaic electrodes commonly use activated carbon as the capacitive component and battery electrode materials as the faradaic (diffusion-limited) component, such as lithium-based oxides (e.g., $LiFePO_4$, $LiMn_2O_4$, $Li_4Ti_5O_{12}$, $Li_2Ti_3O_7$, $LiCrTiO_4$, and $LiTi_2(PO_4)_3$). For instance, Cericola et al. [65] varied the mass ratio of activated carbon to $LiMn_2O_4$ in a hybrid electrode, demonstrating that mixed capacitive and faradaic behavior can be smoothly tuned (Example 4). Böckenfeld et al. [66] demonstrated a hybrid electrode based on $LiFePO_4$ in activated carbon, where the $LiFePO_4$ content was dominant at 65 wt.%. Due to the higher ratio of the faradaic diffusion-limited component, the charge-discharge curves show the typical potential plateau that is associated with battery-type materials. However, the added activated carbon contributed to the specific capacity of the electrode, resulting in 140 mAh g^{-1}, which is an increase of 20 mAh g^{-1} in comparison to the pure oxide material. A similar observation was made by Zhao et al. [67] by mixing multi-walled carbon nanotubes (<10 wt.%) with $Li_4Ti_5O_{12}$, prepared by electrostatic self-assembly, to enhance the rate performance of the battery electrode. The hybrid material showed very high cycling rates while reaching specific capacities of 90 mAh g^{-1} at 90 C and 150 mAh g^{-1} at 5 C [66,67].

5.3. *Electrodes blending pseudocapacitive and capacitive charge storage*

Electrodes blending pseudocapacitive and capacitive charge storage materials are less common since the composite combines typical capacitor characteristics such as high specific power. Huang et al. [68] and Chen et al. [69] synthesized composites with high surface areas and short ion transport paths by combining graphene with nanoplate-MnO_2 and graphene oxide with needle-like MnO_2 nanocrystals, respectively, in an aqueous 1 M Na_2SO_4 electrolyte. The combination of high-surface area graphene and MnO_2, which is a common pseudocapacitive material due to surface redox reactions, delivers a capacitor-like response that is reflected in its high specific capacitance of over 300 F g^{-1} (graphene alone has ca. 50 F g^{-1}) [68] and a CV curve shape that has an almost ideal box-shape. Due to the pseudocapacitive contribution, the CV scan shows hints of current waves. MnO_2 has a pseudocapacitive charge storage mechanism that is faradaic in nature but is not diffusion-limited over the experimental conditions; because of the true faradaic contribution, the reported specific capacitance >300 F g^{-1} must be interpreted cautiously as a 'capacitance' can theoretically only be assigned to a pure capacitive material (see "C_{pseudo}" discussion above). On the other hand, it should not be neglected that the pseudocapacitive material contributes to the specific energy of the hybrid electrode due to its faradaic nature.

6. Conclusions

This review provides (a) an overview of the different types of charge storage mechanisms present in electrochemical energy storage systems, (b) a clear definition of pseudocapacitance and a quantitative framework for distinguishing it from (diffusion-limited) faradaic charge storage processes based on an electrochemical Damköhler number, Da_{el}, (c) a tutorial on how to identify and quantitatively disentangle faradaic, pseudocapacitive, and capacitive charge storage using common electrochemical methods, and (d) a description of representative electrochemical energy storage systems that combine battery, capacitor and

pseudocapacitor characteristics. Furthermore, in the Supplementary Information, we provide detailed step-by-step guides and easy-to-use scripts to disentangle the different charge storage mechanisms using the electrochemical methods discussed here.

Researchers are urged to understand and analyze the different charge storage mechanisms in their own systems and, subsequently, use this understanding to design and control materials and devices that bridge the gap between high specific energy and power at a target cycle life. Correctly identifying and quantifying the charge storage mechanisms involves additional measurements and analyses, but it is of the utmost importance for understanding how the system functions and tuning material properties for specific applications.

Declaration of Competing Interest

The authors declare that they have no known competing financial interests or personal relationships that could have appeared to influence the work reported in this paper.

Acknowledgements

T.S., L.W.G., and R.J.M. gratefully acknowledge funding from the U. S. National Aeronautics and Space Administration (NASA) via the NASA-CCNY Center for Advanced Batteries for Space under cooperative agreement no. 80NSSC19M0199 and the U.S. National Science Foundation (NSF) under CAREER award no. CBET-1847552. D.M. acknowledges support from the Israel National Center for Electrochemical Propulsion (INREP) and the Israel Science Foundation-Chinese National Science Foundation (ISF-CNSF) program under award no. 3650/21. The authors thank Arne Jannaschk for providing the open-source JavaScript to separate diffusion-limited and non-diffusion-limited charge storage contributions.

Supplementary materials

Supplementary material associated with this article can be found, in the online version, at doi:10.1016/j.electacta.2022.140072.

References

[1] T. Reddy, Linden's Handbook of Batteries, 4th ed., McGraw-Hill Education, 2010.
[2] A.J. Bard, L.R. Faulkner, Electrochemical methods. Fundamentals and Applications, Wiley, 2000.
[3] R.G. Compton, C.E. Banks, Understanding Voltammetry, (3rd ed.), World Scientific Publishing Company, 2018.
[4] B.E. Conway, Electrochemical Supercapacitors: Scientific Fundamentals and Technological Applications, Springer, US, 2013.
[5] T.S. Mathis, N. Kurra, X. Wang, D. Pinto, P. Simon, Y. Gogotsi, Energy storage data reporting in perspective-guidelines for interpreting the performance of electrochemical energy storage systems, Adv. Energy Mater. 9 (39) (2019), 1902007.
[6] T. Brousse, D. Bélanger, J.W. Long, To be or not to be pseudocapacitive? J. Electrochem. Soc. 162 (5) (2015) A5185–A5189.
[7] S. Ardizzone, G. Fregonara, S. Trasatti, Inner" and "outer" active surface of RuO_2 electrodes, Electrochim. Acta 35 (1) (1990) 263–267.
[8] J. Wang, J. Polleux, J. Lim, B. Dunn, Pseudocapacitive contributions to electrochemical energy storage in TiO_2 (anatase) nanoparticles, J. Phys. Chem. C 111 (40) (2007) 14925–14931.
[9] A. Lasia, Electrochemical Impedance Spectroscopy and its Applications, Springer, New York, 2014.
[10] S. Fleischmann, J.B. Mitchell, R. Wang, C. Zhan, D. Jiang, V. Presser, V. Augustyn, Pseudocapacitance: from fundamental understanding to high power energy storage materials, Chem. Rev. 120 (14) (2020) 6738–6782.
[11] J. Newman, K.E. Thomas-Alyea, Electrochemical Systems, Wiley, 2004.
[12] L.F. Arenas, C. Ponce de León, F.C. Walsh, Engineering aspects of the design, construction and performance of modular redox flow batteries for energy storage, J. Energy Storage 11 (2017) 119–153.
[13] J. Tafel, Über die polarisation bei kathodischer wasserstoffentwicklung, Z. Phys. Chem. 50U (1) (1905) 641–712.
[14] P. Bai, M.Z. Bazant, Charge transfer kinetics at the solid–solid interface in porous electrodes, Nat. Commun. 5 (1) (2014) 3585.
[15] P. Bai, M.Z. Bazant, Charge transfer kinetics in $LiFePO_4$ porous electrodes: Butler-Volmer equation vs Marcus theory, in: Proceedings of the ECS Meeting Abstracts, 2014.
[16] R.A. Marcus, On the theory of oxidation-reduction reactions involving electron transfer. I, J. Chem. Phys. 24 (5) (1956) 966–978.
[17] R.A. Marcus, On the theory of electron-transfer reactions. VI. Unified treatment for homogeneous and electrode reactions, J. Chem. Phys. 43 (2) (1965) 679–701.
[18] R.J. Brodd, Batteries for Sustainability. Selected Entries from the Encyclopedia of Sustainability Science and Technology, Springer, New York, 2012.
[19] D.C. Grahame, The electrical double layer and the theory of electrocapillarity, Chem. Rev. 41 (3) (1947) 441–501.
[20] V. Augustyn, P. Simon, B. Dunn, Pseudocapacitive oxide materials for high-rate electrochemical energy storage, Energy Environ. Sci. 7 (5) (2014) 1597–1614.
[21] Y. Zhou, P. Jin, Y. Zhou, Y. Zhu, High-performance symmetric supercapacitors based on carbon nanotube/graphite nanofiber nanocomposites, Sci. Rep. 8 (1) (2018) 9005.
[22] N. Elgrishi, K.J. Rountree, B.D. McCarthy, E.S. Rountree, T.T. Eisenhart, J. L. Dempsey, A practical beginner's guide to cyclic voltammetry, J. Chem. Educ. 95 (2) (2018) 197–206.
[23] R.G. Compton, E. Laborda, K.R. Ward, Understanding voltammetry. Simulation of Electrode Processes, Imperial College Press, 2014.
[24] R.Y. Liu, J.J. Chen, Z.W. Li, Q. Ding, X.S. An, Y. Pan, Z. Zheng, M.W. Yang, D.J. Fu, Preparation of $LiFePO_4$/C cathode materials via a green synthesis route for lithium-ion battery applications, Materials 11 (11) (2018) 13.
[25] X. Zhao, Y. Hou, Y. Wang, L. Yang, L. Zhu, R. Cao, Z. Sha, Prepared MnO_2 with different crystal forms as electrode materials for supercapacitors: experimental research from hydrothermal crystallization process to electrochemical performances, RSC Adv. 7 (64) (2017) 40286–40294.
[26] H. Lindström, S. Södergren, A. Solbrand, H. Rensmo, J. Hjelm, A. Hagfeldt, S. E. Lindquist, Li+ Ion Insertion in TiO_2 (Anatase). 2. Voltammetry on nanoporous films, J. Phys. Chem. B 101 (39) (1997) 7717–7722.
[27] J.B. Cook, H.S. Kim, T.C. Lin, C.H. Lai, B. Dunn, S.H. Tolbert, Pseudocapacitive charge storage in thick composite MoS_2 nanocrystal-based electrodes, Adv. Energy Mater. 7 (2) (2017), 1601283.
[28] J.H. Xu, D.E. Turney, A.L. Jadhav, R.J. Messinger, Effects of graphite structure and ion transport on the electrochemical properties of rechargeable aluminum-graphite batteries, ACS Appl. Energy Mater. 2 (11) (2019) 7799–7810.
[29] Y. Yan, B. Hao, D. Wang, G. Chen, E. Markweg, A. Albrecht, P. Schaaf, Understanding the fast lithium storage performance of hydrogenated TiO_2 nanoparticles, J. Mater. Chem. A 1 (46) (2013) 14507–14513.
[30] E. Lim, C. Jo, H. Kim, M.H. Kim, Y. Mun, J. Chun, Y. Ye, J. Hwang, K.S. Ha, K. C. Roh, K. Kang, S. Yoon, J. Lee, Facile synthesis of Nb_2O_5@carbon core–shell nanocrystals with controlled crystalline structure for high-power anodes in hybrid supercapacitors, ACS Nano 9 (7) (2015) 7497–7505.
[31] H.S. Kim, J.B. Cook, H. Lin, J.S. Ko, S.H. Tolbert, V. Ozolins, B. Dunn, Oxygen vacancies enhance pseudocapacitive charge storage properties of MoO_{3-x}, Nat. Mater. 16 (4) (2017) 454–460.
[32] T. Schoetz, M. Kurniawan, M. Stich, R. Peipmann, I. Efimov, A. Ispas, A. Bund, C. Ponce de Leon, M. Ueda, Understanding the charge storage mechanism of conductive polymers as hybrid battery-capacitor materials in ionic liquids by *in situ* atomic force microscopy and electrochemical quartz crystal microbalance studies, J. Mater. Chem. A 6 (36) (2018) 17787–17799.
[33] J.H. Xu, T. Schoetz, J.R. McManus, V.R. Subramanian, P.W. Fields, R.J. Messinger, Tunable pseudocapacitive intercalation of chloroaluminate anions into graphite electrodes for rechargeable aluminum batteries, J. Electrochem. Soc. 168 (6) (2021), 060514.
[34] M.D. Levi, E. Markevich, D. Aurbach, Comparison between Cottrell diffusion and moving boundary models for determination of the chemical diffusion coefficients in ion-insertion electrodes, Electrochim. Acta 51 (1) (2005) 98–110.
[35] H.C. Shin, S.I. Pyun, The kinetics of lithium transport through $Li1-\delta CoO_2$ by theoretical analysis of current transient, Electrochim. Acta 45 (3) (1999) 489–501.
[36] H.C. Shin, S.I. Pyun, An investigation of the electrochemical intercalation of lithium into a $Li1-\delta CoO_2$ electrode based upon numerical analysis of potentiostatic current transients, Electrochim. Acta 44 (13) (1999) 2235–2244.
[37] S. Ghosh, R. Santhosh, S. Jeniffer, V. Raghavan, G. Jacob, K. Nanaji, P. Kollu, S. K. Jeong, A.N. Grace, Natural biomass derived hard carbon and activated carbons as electrochemical supercapacitor electrodes, Sci. Rep. 9 (1) (2019) 16315.
[38] M. Miroshnikov, K.P. Divya, G. Babu, A. Meiyazhagan, L.M. Reddy Arava, P. M. Ajayan, G. John, Power from nature: designing green battery materials from electroactive quinone derivatives and organic polymers, J. Mater. Chem. A 4 (32) (2016) 12370–12386.
[39] K. Fic, A. Platek, J. Piwek, E. Frackowiak, Sustainable materials for electrochemical capacitors, Mater. Today 21 (4) (2018) 437–454.
[40] X.D. Ren, Y.Y. Wu, A low-overpotential potassium-oxygen battery based on potassium superoxide, J. Am. Chem. Soc. 135 (8) (2013) 2923–2926.
[41] P. Córdoba-Torres, T.J. Mesquita, R.P. Nogueira, Relationship between the origin of constant-phase element behavior in electrochemical impedance spectroscopy and electrode surface structure, J. Phys. Chem. C 119 (8) (2015) 4136–4147.
[42] P.L. Taberna, P. Simon, J.F. Fauvarque, Electrochemical characteristics and impedance spectroscopy studies of carbon-carbon supercapacitors, J. Electrochem. Soc. 150 (3) (2003) A292.
[43] J.S. Ko, C.H. Lai, J.W. Long, D.R. Rolison, B. Dunn, J. Nelson Weker, Differentiating double-layer, psuedocapacitance, and battery-like mechanisms by analyzing impedance measurements in three dimensions, ACS Appl. Mater. Interfaces 12 (12) (2020) 14071–14078.
[44] V. Augustyn, J. Come, M.A. Lowe, J.W. Kim, P.L. Taberna, S.H. Tolbert, H. D. Abruña, P. Simon, B. Dunn, High-rate electrochemical energy storage through Li + intercalation pseudocapacitance, Nat. Mater. 12 (6) (2013) 518–522.

[45] Y.L. Shao, M.F. El-Kady, J.Y. Sun, Y.G. Li, Q.H. Zhang, M.F. Zhu, H.Z. Wang, B. Dunn, R.B. Kaner, Design and mechanisms of asymmetric supercapacitors, Chem. Rev. 118 (18) (2018) 9233–9280.
[46] Y.L. Huang, Y.X. Zeng, M.H. Yu, P. Liu, Y.X. Tong, F.L. Cheng, X.H. Lu, Recent smart methods for achieving high-energy asymmetric supercapacitors, Small Methods 2 (2) (2018) 1700230.
[47] S.H. Zheng, Z.S. Wu, S. Wang, H. Xiao, F. Zhou, C.L. Sun, X.H. Bao, H.M. Cheng, Graphene-based materials for high-voltage and high-energy asymmetric supercapacitors, Energy Storage Mater. 6 (2017) 70–97.
[48] N. Choudhary, C. Li, J. Moore, N. Nagaiah, L. Zhai, Y. Jung, J. Thomas, Asymmetric supercapacitor electrodes and devices, Adv. Mater. 29 (21) (2017) 1605336.
[49] J.F. Sun, C. Wu, X.F. Sun, H. Hu, C.Y. Zhi, L.R. Hou, C.Z. Yuan, Recent progresses in high-energy-density all pseudocapacitive-electrode-materials-based asymmetric supercapacitors, J. Mater. Chem. A 5 (20) (2017) 9443–9464.
[50] M.H. Yu, Z.L. Wang, Y. Han, Y.X. Tong, X.H. Lu, S.H. Yang, Recent progress in the development of anodes for asymmetric supercapacitors, J. Mater. Chem. A 4 (13) (2016) 4634–4658.
[51] F.X. Wang, S.Y. Xiao, Y.Y. Hou, C.L. Hu, L.L. Liu, Y.P. Wu, Electrode materials for aqueous asymmetric supercapacitors, RSC Adv. 3 (32) (2013) 13059–13084.
[52] R.R. Salunkhe, J. Tang, Y. Kamachi, T. Nakato, J.H. Kim, Y. Yamauchi, Asymmetric supercapacitors using 3D nanoporous carbon and cobalt oxide electrodes synthesized from a single metal-organic framework, ACS Nano 9 (6) (2015) 6288–6296.
[53] J.W. Long, D. Belanger, T. Brousse, W. Sugimoto, M.B. Sassin, O. Crosnier, Asymmetric electrochemical capacitors-Stretching the limits of aqueous electrolytes, MRS Bull. 36 (7) (2011) 513–522.
[54] P.C. Chen, G.Z. Shen, Y. Shi, H.T. Chen, C.W. Zhou, Preparation and characterization of flexible asymmetric supercapacitors based on transition-metal-oxide nanowire/single-walled carbon nanotube hybrid thin-film electrodes, ACS Nano 4 (8) (2010) 4403–4411.
[55] L. Kavan, M. Kalbáč, M. Zukalová, I. Exnar, V. Lorenzen, R. Nesper, M. Graetzel, Lithium storage in nanostructured TiO_2 Made by hydrothermal growth, Chem. Mater. 16 (3) (2004) 477–485.
[56] T. Brezesinski, J. Wang, J. Polleux, B. Dunn, S.H. Tolbert, Templated nanocrystal-based porous TiO_2 films for next-generation electrochemical capacitors, J. Am. Chem. Soc. 131 (5) (2009) 1802–1809.
[57] M. Okubo, E. Hosono, J. Kim, M. Enomoto, N. Kojima, T. Kudo, H. Zhou, I. Honma, Nanosize effect on high-rate Li-ion intercalation in $LiCoO_2$ electrode, J. Am. Chem. Soc. 129 (23) (2007) 7444–7452.
[58] B.K. Lesel, J.B. Cook, Y. Yan, T.C. Lin, S.H. Tolbert, Using nanoscale domain size to control charge storage kinetics in pseudocapacitive nanoporous $LiMn_2O_4$ powders, ACS Energy Lett. 2 (10) (2017) 2293–2298.
[59] B.K. Lesel, J.S. Ko, B. Dunn, S.H. Tolbert, Mesoporous $LixMn_2O_4$ thin film cathodes for lithium-ion pseudocapacitors, ACS Nano 10 (8) (2016) 7572–7581.
[60] H. Marsh, F.R. Reinoso, Activated Carbon, Elsevier Science, 2006.
[61] L.M. Dai, Functionalization of graphene for efficient energy conversion and storage, Acc. Chem. Res. 46 (1) (2013) 31–42.
[62] P.C. Chen, G. Shen, Y. Shi, H. Chen, C. Zhou, Preparation and characterization of flexible asymmetric supercapacitors based on transition-metal-oxide nanowire/single-walled carbon nanotube hybrid thin-film electrodes, ACS Nano 4 (8) (2010) 4403–4411.
[63] G. Wu, P. Tan, D. Wang, Z. Li, L. Peng, Y. Hu, C. Wang, W. Zhu, S. Chen, W. Chen, High-performance supercapacitors based on electrochemical-induced vertical-aligned carbon nanotubes and polyaniline nanocomposite electrodes, Sci. Rep. 7 (2017) 43676.
[64] S. Venkateshalu, A.N. Grace, Review-heterogeneous 3D graphene derivatives for supercapacitors, J. Electrochem. Soc. 167 (5) (2020) 050509.
[65] D. Cericola, P. Novák, A. Wokaun, R. Kötz, Segmented bi-material electrodes of activated carbon and $LiMn_2O_4$ for electrochemical hybrid storage devices: Effect of mass ratio and C-rate on current sharing, Electrochim. Acta 56 (3) (2011) 1288–1293.
[66] N. Böckenfeld, R.S. Kühnel, S. Passerini, M. Winter, A. Balducci, Composite $LiFePO_4$/AC high rate performance electrodes for Li-ion capacitors, J. Power Sources 196 (8) (2011) 4136–4142.
[67] S. Zhao, M. Zhang, Z. Wang, X. Xian, Enhanced high-rate performance of $Li_4Ti_5O_{12}$ microspheres/multiwalled carbon nanotubes composites prepared by electrostatic self-assembly, Electrochim. Acta 276 (2018) 73–80.
[68] H. Huang, X. Wang, Graphene nanoplate-MnO_2 composites for supercapacitors: a controllable oxidation approach, Nanoscale 3 (8) (2011) 3185–3191.
[69] S. Chen, J. Zhu, X. Wu, Q. Han, X. Wang, Graphene oxide-MnO_2 nanocomposites for supercapacitors, ACS Nano 4 (5) (2010) 2822–2830.